AD-A049 581 FAIRCHILD REPUBLIC CO FARMINGDALE N Y F/G 17/2.1
PULSED PLASMA RADIO FREQUENCY INTERFERENCE STUDIES.(U)
SEP 77 M BEGUN, W GUNMAN F04611-76-0057
UNCLASSIFIED AFRPL-TR-77-85 NL

| OF |
AD
A049581

END
DATE
FILMED
3-78
DDC

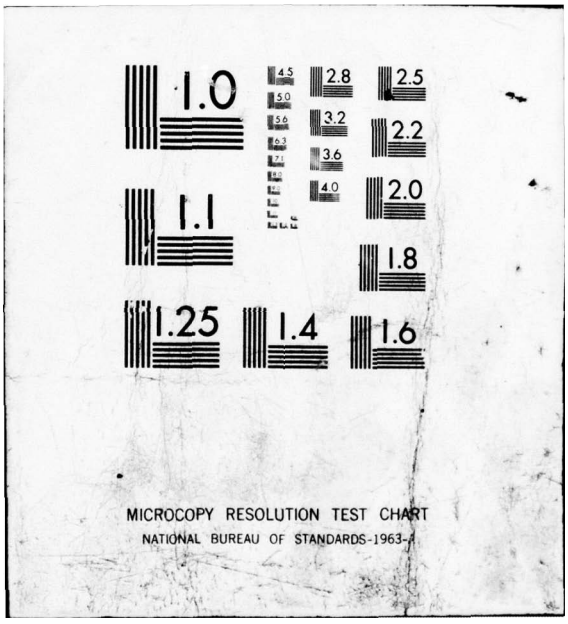
1.0
1.1
1.25
1.4
1.6
1.8
2.0
2.2
2.5
2.8
3.2
3.6
4.0
4.5
5.0
5.6
6.3
7.1
8.0
MICROCOPY RESOLUTION TEST CHART
NATIONAL BUREAU OF STANDARDS-1963-A

AD A049581

AFRPL-TR-77-85

PULSED PLASMA RADIO FREQUENCY INTERFERENCE STUDIES

FINAL REPORT FOR PERIOD 17 JUNE 1976 - 1 SEPTEMBER 1977

AUTHORS: MARTIN BEGUN
WILLIAM J. GUMAN

SEPTEMBER 1977

FAIRCHILD INDUSTRIES, INC.
FAIRCHILD REPUBLIC COMPANY
FARMINGDALE, N.Y. 11735

AD No. _____
DDC FILE COPY

APPROVED FOR PUBLIC RELEASE
DISTRIBUTION UNLIMITED

AIR FORCE ROCKET PROPULSION LABORATORY
DIRECTOR OF SCIENCE AND TECHNOLOGY
AIR FORCE SYSTEMS COMMAND
EDWARDS, CALIFORNIA 93523

DDC
RECEIVED
FEB 3 1978
D

NOTICE

When Government drawings, specifications, or other data are used for any purpose other than in connection with a definitely related Government procurement operation the United States Government thereby incurs no responsibility nor any obligation whatsoever; and the fact that the Government may have formulated, furnished, or in any way supplied the said drawings, specifications, or other data, is not to be regarded by implication or toherwise as in any manner licensing the holder or any other person or corporation, or conveying any rights or permission to manufacture, use, or sell any patented invention that may in any way be related thereto.

FOREWORD

This final report was prepared by Fairchild Industries, Inc., Fairchild Republic Company under Air Force Contract F04611-76-C-0057, Job Order Number 305812 PL "Pulsed Plasma Radio Frequency Interference Studies".

The research reported upon was supported by the Air Force Rocket Propulsion Laboratory. The program was monitored in the Liquid Rocket Division originally by 1st Lt Sharon A. Pruitt and subsequently by Capt Gregory A. Engelbreit.

Work on this contract began in June 1976 and was completed in August 1977 and the pertinent studies of this period are reported herein. This report was submitted by the authors in September 1977.

The authors wish to acknowledge the overall contributions of Mr M. Katchmar as well as the assistance of Messrs. S. Pasternak and F. Carlson in the Laboratory effort. Their combined skilled craftsmanship and many meaningful suggestions were a significant factor to the success of this effort. Specific acknowledgment is made to Mr S. Burruano, as consultant, for his valuable contributions in the analysis and RFI testing phase of this program.

This report has been reviewed by the Information Office/DOZ and is releasable to the National Technical Information Service (NTIS). At NTIS it will be available to the general public, including foreign nations. This technical report has been reviewed and is approved for publication; it is unclassified and suitable for general public release.

Michael R Brasher

MICHAEL R. BRASHER, Lt
Project Manager

Thomas W. Waddell

THOMAS W. WADDELL, Chief
Satellite Propulsion Section

FOR THE COMMANDER

Edward E Stein

EDWARD E. STEIN
Deputy Chief, Liquid Rocket Division

UNCLASSIFIED

SECURITY CLASSIFICATION OF THIS PAGE (When Data Entered)

(19) REPORT DOCUMENTATION PAGE

READ INSTRUCTIONS BEFORE COMPLETING FORM

(18) 1. REPORT NUMBER: AFRPL-TR-77-85

2. GOVT ACCESSION NO.

3. RECIPIENT'S CATALOG NUMBER

(6) 4. TITLE (and Subtitle): Pulsed Plasma Radio Frequency Interferehce Studies.

5. TYPE OF REPORT & PERIOD COVERED: (9) FINAL repts, 17 Jun[illegible]976 - 1 Sept[illegible]77

6. PERFORMING ORG. REPORT NUMBER

(10) 7. AUTHOR(s): Martin Begun, William Guman

(15) 8. CONTRACT OR GRANT NUMBER(s): F04611-76-C-0057

9. PERFORMING ORGANIZATION NAME AND ADDRESS: Fairchild Republic Company, Farmingdale, New York 11735

(12) 53 p.

10. PROGRAM ELEMENT, PROJECT, TASK AREA & WORK UNIT NUMBERS: 02302F, 3058, (16) JON 305812PL

11. CONTROLLING OFFICE NAME AND ADDRESS: AF Rocket Propulsion Laboratory (AFSC), Director of Science and Technology, Edwards AFB, California 93523

(11)

12. REPORT DATE: Sept[illegible]977 (17)

13. NUMBER OF PAGES: 47

14. MONITORING AGENCY NAME & ADDRESS (if different from Controlling Office): Same as Item 11. above

15. SECURITY CLASS. (of this report): UNCLASSIFIED

15a. DECLASSIFICATION/DOWNGRADING SCHEDULE

16. DISTRIBUTION STATEMENT (of this Report)

Approved for Public Release
Distribution Unlimited

17. DISTRIBUTION STATEMENT (of the abstract entered in Block 20, if different from Report)

18. SUPPLEMENTARY NOTES

None

62302F

19. KEY WORDS (Continue on reverse side if necessary and identify by block number)

Electric Propulsion
Plasma Propulsion
Space Propulsion
Radio Frequency Interference
Spacecraft Integration

20. ABSTRACT (Continue on reverse side if necessary and identify by block number)

An unshielded external test set was developed which allows the millipound thrust level pulsed plasma thruster to be repetitvely operated in air. The present design was operated at a peak discharge current of 47 kiloamperes.

Electromagnetic emission tests carried out showed that the present unshielded test set would have to be shielded if the pulsed noise generated by it has to meet RE02 electric field and magnetic field requirements. The results of the noise measurements presented can be used as a basis for the design of the shielding.

Shielding effectiveness measurements have shown that EMI gaskets are not required in the covers of the thruster enclosure if the covers are well fitted and secured by a double row of alternately spaced screws.

DD FORM 1 JAN 73 1473 EDITION OF 1 NOV 65 IS OBSOLETE S/N 0102-014-6601 |

UNCLASSIFIED

SECURITY CLASSIFICATION OF THIS PAGE (When Data Entered)

408 278

CONTENTS

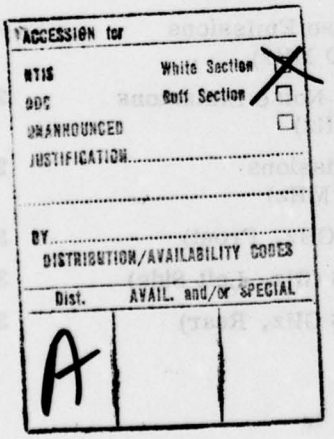

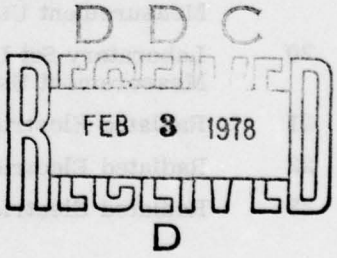

ILLUSTRATIONS

ILLUSTRATIONS (Cont)

1.0 INTRODUCTION

The results of RFI testing of a Pulsed Plasma Thruster were presented in a previous report.[1]

The objectives of the present program were two-fold. The first objective was to fabricate and optimize for minimum radio frequency interference a one millipound thrust level solid propellent pulsed plasma thruster. This objective was met by designing an EMI secure enclosure to contain the millipound thrust level pulsed plasma thruster cited above. The technique pursued was to be consistent with the ability to utilize the design approach in future flight hardware. Two approaches were investigated for this purpose:

1) The use of enclosure covers with machined grooves containing knitted metal gaskets, and
2) The use of gasketless, well fitted, covers with closely spaced screws to secure the covers to a structural frame of the thruster.

The second objective of the program was to develop a test set which would allow the thruster to be operated in air. Such a test set will greatly simplify the integration of a pulsed plasma propulsion system into a satellite without requiring a specialized vacuum facility. In this capacity, the test set allows the user to exercise the thruster during integration and also allows the user to check the compatibility of the thruster with other satellite systems with respect to electromagnetic noise. No attempt was made in the present study to provide EMI shielding for the test set.

The testing carried out in this program with the thruster and test set generated experimental data which can be used for an independent shielding analysis in the event it is necessary to have a test set which meets the specification limits of MIL-STD-1541.

2.0 THRUSTER ENCLOSURE SHIELDING STUDY

2.1 Description of Enclosure Covers

The enclosure surrounding the thruster consists of an accurately welded and machined rectangular frame of aluminum angles onto which flat sheet metal covers are attached. Figure 1 is a photograph of the partially uncovered enclosure with the test set attached to it. The aluminum covers have been machined so that a close fit exists between them and the frame. The screws which hold the covers in place are spaced 3.4 cm (1.3 in) apart, and two staggered rows of screws are used. This mounting approach is followed over all the edges of the thruster enclosure (See Figure 1). The cover panels of the enclosure are made of 0.1 cm (40 mil) aluminum. This thickness corresponds to a few skin depths at the lower R. F. frequencies of interest.

The R. F. seal for these covers is a custom designed gasket (Model 91-02602) made of knitted aluminum wire manufactured by Technical Wire Products, Cranford, New Jersey.

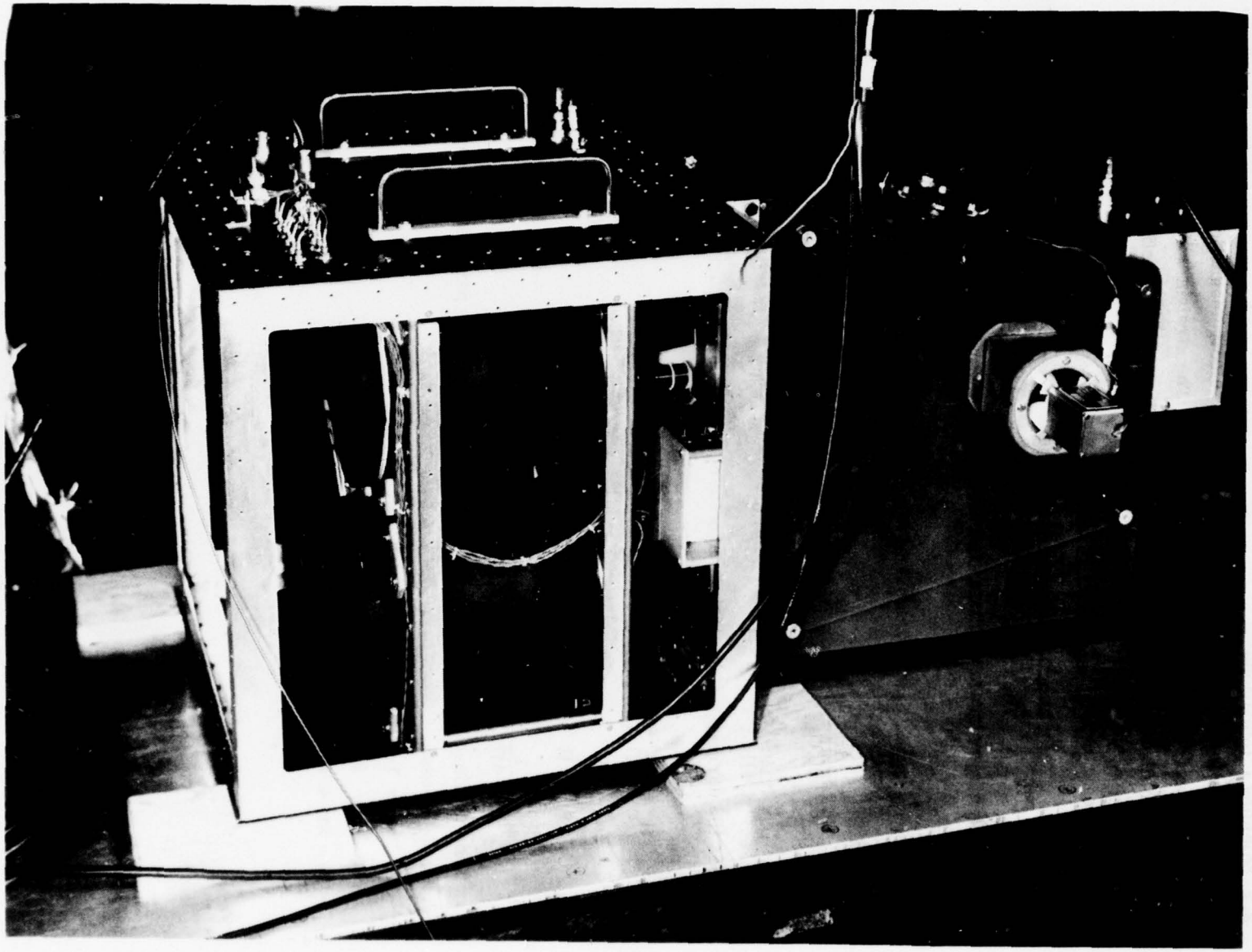

Figure 1. Test Set Attached to Uncovered Thruster

2.2 Shielding Calculations

The basis for the shielding calculations are the electromagnetic fields of a straight current element, and the fields of a current loop. The straight wire source is equivalent to an electric dipole of moment $|p| = \frac{IS}{\omega}$, and the loop to a magnetic dipole of moment $|m| = IA$

where I = Current

S = Length of the current element

A = The area of the loop

The electromagnetic equations for the current element in a polar coordinate system are:[2]

$$E_r = \frac{1}{2\Pi\epsilon_o}\left(\frac{1}{r^3} - \frac{ik}{r^2}\right)\cos\theta\,|p|\,e^{i(kr-\omega t)}$$

$$E_\theta = \frac{1}{4\Pi\epsilon_o}\left(\frac{1}{r^3} - \frac{ik}{r^2} - \frac{k^2}{r}\right)\sin\theta\,|p|\,e^{i(kr-\omega t)}$$

$$H_\phi = \frac{-i\omega}{4\Pi}\left(\frac{1}{r^2} - \frac{ik}{r}\right)\sin\theta\,|p|\,e^{i(kr-\omega t)}$$

whereas the corresponding electromagnetic equations for the current loop are:

$$H_r = \frac{1}{2\Pi}\left(\frac{1}{r} - \frac{ik}{r^2}\right)\cos\theta\,|m|\,e^{i(kr-\omega t)}$$

$$E_\phi = \frac{k^2}{4\Pi}\sqrt{\frac{\mu}{\epsilon}}\left(\frac{1}{r} + \frac{i}{kr^2}\right)\sin\theta\,|m|\,e^{i(kr-\omega t)}$$

$$H_\theta = \frac{1}{4\Pi}\left(\frac{1}{r^3} - \frac{ik}{r^2} - \frac{k^2}{r}\right)\sin\theta\,|m|\,e^{i(kr-\omega t)}$$

The equations can be written in the parameter kr. This parameter determines the region of interest.

1) $kr > 1$: The far field region
2) $kr = 1$: The transition region
3) $kr < 1$: The near field region

Substituting for |p| and |m| and taking the real part, one obtains the following two sets of expressions

the Electric Dipole:

$$E_r = \frac{IS\chi k^2}{2\Pi} \cos\theta \left(\frac{\cos\Psi}{(kr)^3} + \frac{\sin\Psi}{(kr)^2} \right)$$

$$E_\theta = \frac{IS\chi k^2 \sin\theta}{4\Pi} \left(\frac{\cos\Psi}{(kr)^3} + \frac{\sin\Psi}{(kr)^2} - \frac{\cos\Psi}{kr} \right)$$

$$H_\phi = \frac{ISk^2 \sin\theta}{4\Pi} \left(\frac{\sin\Psi}{(kr)^2} - \frac{\cos\Psi}{kr} \right)$$

and the Magnetic Dipole:

$$H_r = \frac{IAk^2}{2\Pi} \cos\theta \left(\frac{\cos\Psi}{(kr)^3} + \frac{\sin\Psi}{(kr)^2} \right)$$

$$E_\phi = \frac{IA\chi k^2 \sin\theta}{4\Pi} \left(\frac{-\sin\Psi}{(kr)^2} + \frac{\cos\Psi}{kr} \right)$$

$$H_\theta = \frac{IAk^3 \sin\theta}{4\Pi} \left(\frac{\cos\Psi}{(kr)^3} + \frac{\sin\Psi}{(kr)^2} - \frac{\cos\Psi}{kr} \right)$$

The equations in this form are the basis for the shielding calculations.[3] The use of the electric dipole fields for shielding calculations gives results which are optimistic with respect to the magnetic dipole fields. We will therefore base all of our calculations on the dipole magnetic fields.

We will be concerned mainly with the near field and use the definition of the wave impedance of free space, $Zo = \sqrt{\frac{\mu o}{\epsilon_o}} = 377\Omega$. This expression is obtained by considering the contribution for which $kr \gg 1$. The wave impedance is then defined by E/H. A quantity called the "shielding effectiveness" will now be defined. This quantity is a figure of merit which describes the shielding efficiency of an electromagnetic shield.

$$SE_{dB} = 10 \log_{10} \frac{\text{incident power density}}{\text{transmitted power density}}$$

where 1) incident power density = power density before the shield is in place at the measuring point.

2) transmitted power density = power density at the measuring point after the shield is in place.

In terms of the field, we can write the expressions for $S.E_{dB}$ as:

$$S.E_{dB} = 20 \log_{10} \frac{E_{in}}{E_{tr}} \quad \text{for electric fields}$$

$$S.E_{dB} = 20 \log_{10} \frac{H_{in}}{H_{tr}} \quad \text{for magnetic fields}$$

The complete description of the effect of an impinging electromagnetic field must take account of the multiple scattering properties of the barrier. We can write the transmitted field relative to an incident field of unit strength as:

$$E_{tr} = e^{-\alpha t} \frac{4K}{(1+K)^2} \left(1 - \left(\frac{K-1}{K+1} \right)^2 e^{-2\gamma t} \right)^{-1}$$

Hence,

$$S.E_{dB} = 20 \log_{10} \frac{1}{E_{tr}}$$

$$= 20 \log_{10} \left(e^{\alpha t} \frac{(1+K)^2}{4K} \left| 1 - \left(\frac{K-1}{K+1} \right)^2 e^{-2\gamma t} \right| \right)$$

This is usually written as:

$$S.E_{db} = A_{dB} + R_{dB} + B_{dB}$$

where $A_{dB} = 8.686\, \alpha t$ (absorption loss)

$$R_{dB} = 20 \log_{10} \frac{(1+K)^2}{4K} \quad \text{(reflection loss)}$$

$$B_{dB} = 20 \log_{10} \left(1 - \left(\frac{K-1}{K+1} \right)^2 e^{-2\gamma t} \right) \quad \text{re-reflection correction}$$

The quantity γ is the propagation constant and is equal to $\gamma = \alpha + i\,\beta = i\,\omega\,\mu\,(\sigma + i\,\omega\,\epsilon)$ and for metals $\sigma >> \omega\epsilon$ This implies that $\alpha = \beta = 1/\sqrt{2}\,(\sqrt{\omega\mu\sigma})$ where μ is the permeability of the material and σ is the conductivity.

A common convention is to reference the constants of the material to copper, and to measure the frequency in MHz.

We can then write the constants as

$$\tau = \tau_c\, \tau_r$$

$$\mu = \mu_c\, \mu_r$$

where μ_c = permeability of copper = 1

μ_r = the value of the material relative to copper.

The absorption loss can now be written

as $A_{dB} = 1314.3t\sqrt{\mu_r \sigma_r f_{MHZ}}$ with t in cm

or, $A_{dB} = 3.338t\sqrt{\mu_r \sigma_r f_{MHZ}}$ with t in mils

In a similar fashion, one can present the reflection term and re-reflection term in a more convenient form. For calculational purposes, we will calculate the total loss. The value of K is given by $K = 22r\sqrt{f}$, where f is in Hz, and r is in meters. For the parameters of interest $K \gg 1$ for electric or magnetic dipole sources. We can write the loss as

$$S.E_{dB} = 20 \log_{10}\left(e^{\alpha t}\ \frac{(1+K)^2}{4K}\ \left|1 - \left(\frac{K-1}{K+1}\right)^2\ e^{-2\gamma t}\right|\right)$$

For $K \gg 1$ this can be written as

$$S.E_{dB} = 20 \log_{10} e^{t/\delta} + 20 \log\left(\left(\frac{K}{4}\right)\left(1 - e^{-2t/\delta}\right)\right)$$

Where we have also assumed that $t/\delta \geq 1$

In the above, t is the shield thickness and δ is the skin depth.

Assuming a magnetic source, we have

$$|K| = 2.14 \times 10^4 r_m \sqrt{\frac{\sigma_r}{\mu_r}\ f_{MHZ}}$$

where r_m is the distance in meters.

Figures 2 and 3 present curves for the S.E. for 40 mil and 20 mil thick aluminum, respectively. There is another figure of merit which is useful where weight sensitive applications are concerned. This factor is called the shielding density, S.D.

$$S.D. = SE_{dB}\ W/A$$

where W/A = weight per unit area of metal of thickness t.

As an example, suppose we require the same S.E., but we wish to find out what thickness of copper would be required for $r_m = 0.1$ meter. The results of the calculation are as follows:

frequency (Mhz)	thickness (mils)	thickness, (Cm)
.01	31.3	0.0795
.1	37	0.094
1	39.5	0.100

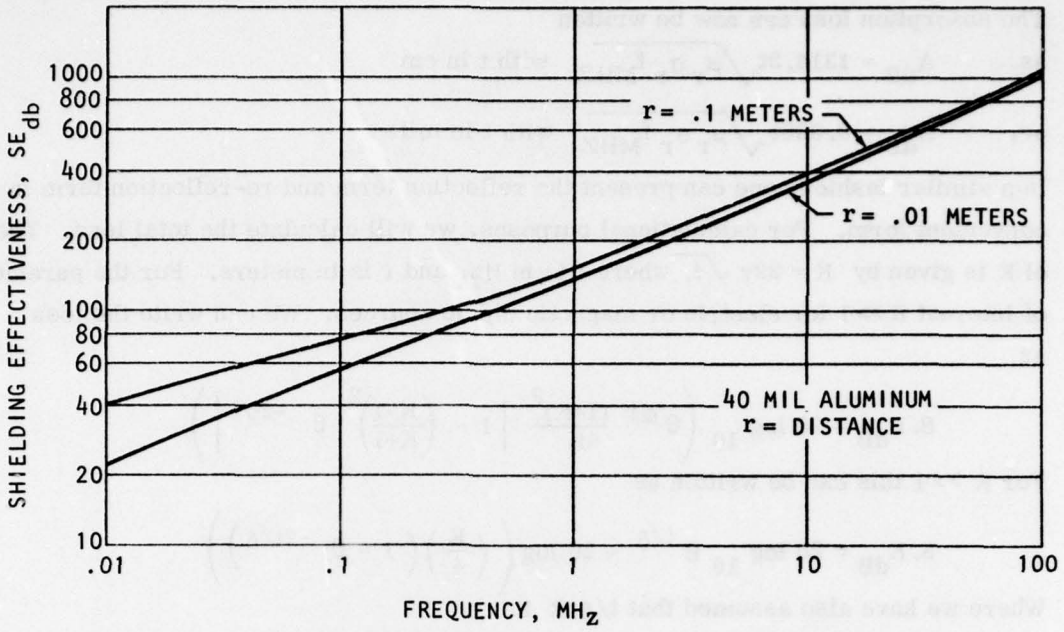

Figure 2. Shielding Effectiveness For 40 Mil Aluminum Barrier

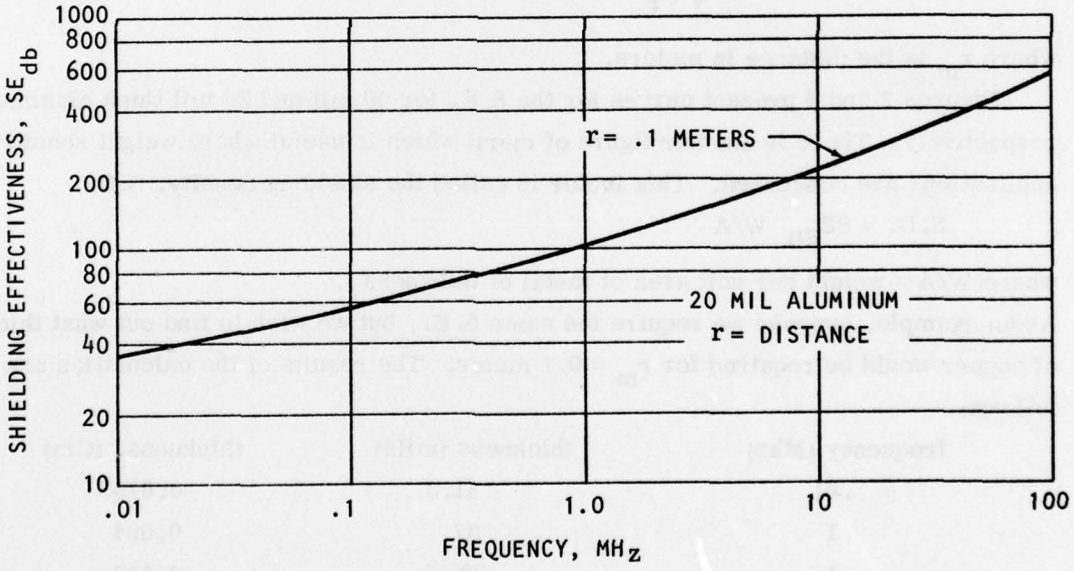

Figure 3. Shielding Effectiveness For 20 mil Aluminum Barrier

The weight ratio for copper to aluminum per mil is 3.29 so for this specific requirement, aluminum is preferred over copper since it is lighter at all frequencies. Under other conditions when one specifies the electromagnetic environment and the S.E. required, one can trade off different materials for mechanical strength versus their electromagnetic properties with the constraint of minimum weight.

2.3 Attenuation Due to a Circular Guide (Air Vent Tube)

The assembled thruster enclosure is a well sealed box. If such a box were subjected to a rapid change in pressure, such as occurs during the launch of a satellite, then large pressure forces could be generated which could possibly distort or even damage the thruster enclosure. We have therefore provided two vent tubes which allow air from the interior of the box to be exhausted. These vent tubes are located on the inside of the enclosure with one of their ports flush with the surface of a cover panel of the box. These vent tubes act as a waveguide for frequencies above its cutoff frequency. For frequencies below cut off, the tube acts as an attenuator of electromagnetic energy. The progation constant for a circular waveguide[4] is $\chi^2 = (P'nm/a)^2 - k_o^2$ for T. E_{nm} modes. where $P'nm$ are the roots of $d\, J_m (k_c r)/dr\big|_{r=a} = O$ and a is the radius of the guide. We choose the T. E_{01} mode since it is one of the 1st modes to propogate. We then obtain $(P'_{01}/a)^2 = (3.832/a)^2 = k_c^2 = (2\pi/\tau_c)^2$. For non-propagating modes, ie $\tau > \tau_c$ we obtain $\chi = 2\pi/\tau_c \sqrt{1 - (\tau_c/\tau)^2}$ for $\tau > \tau_c$ one can expand the square root and obtain $\chi = (2\pi/\tau_c)\left(1 - 1/2\,(\tau_c/\tau)^2\right)$ nepers/meter. In terms of f_{MHZ} and χ in dB/inch this becomes $\chi = 33.3/a\,(1 - 1/2\ a\, f_{MHZ}/7203)$ where the cut-off frequency is $f_{MHZ} = 7203/a$, and a is in inches.

Each vent tube used in the present program has a diameter of 0.46 cm (0.18 in). This size tube leads to a cutoff frequency of 115 GHz and an attenuation of at least 370 db/inch for frequencies which are 16 GHz or lower. The length of the vent tube is 7.62 cm (3 in) so that a high degree of attenuation is realized.

One of the sheet metal covers of the thruster enclosure has twelve 0.635 cm (0.25 in) diameter holes in it to lead out thermistor leads. RF Interonics, Model 320 bypass capacitors have been inserted in these holes as part of the feed through. An estimate can be made of the shielding effectiveness of these holes by calculating the attenuation of a hole considered as a guide beyond cutoff and then adding the attenuation of the bypass capacitors. The thickness of the panel is 0.10 cm (0.040 inches). This thickness gives a χ' of 13 dB. Figure 4 presents a graph of $S.E._{dB}$ for the capacitors plus the hole.

At distances far from the cover panel, the intensity would be roughly that of a single hole multiplied by the number of holes. For frequencies of 100 MHz or less, one would

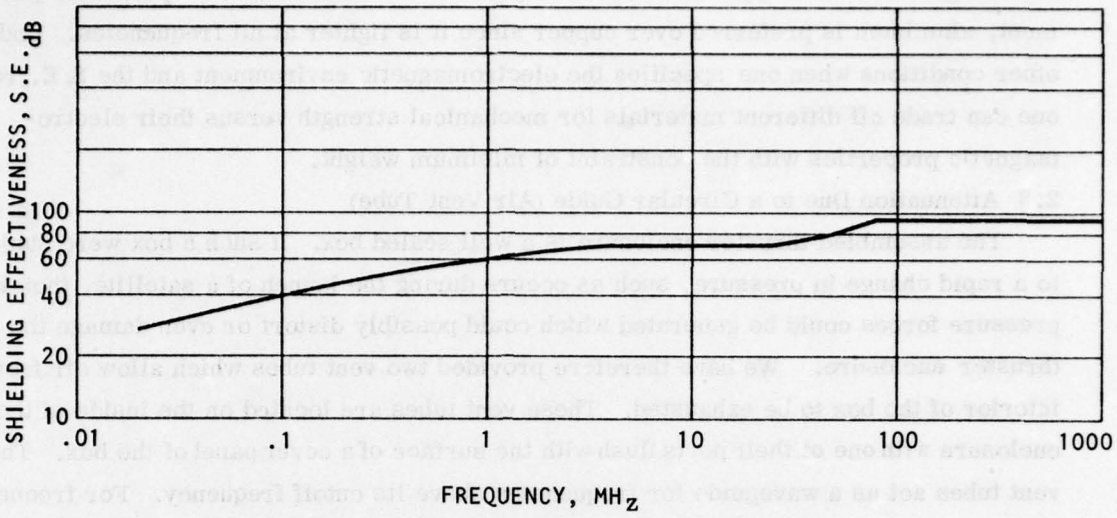

Figure 4. Shielding Effectiveness of Holes Plus Bypass Capacitors

expect that the capacitor plus the cut off guide approximation to hold. For frequencies higher than 100 MHz, but less than the cut off frequency, one can expect a different interference pattern to occur. As a conservative estimate, one can take one hole plus the bypass capacitor and multiply the result by the number of holes to give 73 dB attenuation.

3.0 UNSHIELDED TEST SET

3.1 General Description

The unshielded test set was designed so that it could easily be electrically attached to the thruster electrodes, and also be portable. The electrical characteristics of the unshielded test set were to be such that the discharge current waveform of the assembly would be similar to that generated by the thruster alone in actual operation. The mechanical design of the test set was constrained by the requirement for low inductance and simplicity of connection to the electrodes of the thruster.

The test set's basic structure is that of a rectangular box. This box bolts onto the front lower plate of the thruster enclosure (see Figure 1). This technique provides the mechanical support for the test set to the thruster. The interior of the box of the test set (see Figure 7) contains an electrical stripline assembly for the discharge current, a resistive load, and a triggered gap switch. External to the box are the accessories such as a fan for cooling the resistive load, a volt meter for monitoring the voltage on the thruster capacitor tank, and the triggering circuit for the spark gap switch. This

arrangement allows for safe operation. Figures 5, 6 and 7 present different views of the test set. Figure 1 is a photograph showing the test set connected to the thruster.

3.2 Electrical Design

The underlying electrical design of the test set took into account the desirability of seeking to simulate the actual operation of a thruster with regard to peak discharge current amplitude and waveform. This feature of the test set would enable it also to be used for the testing of energy storage capacitors under their full current capabilities.

In its present configuration, the test set maximum current is somewhat less than obtained when the thruster is operated without the test set attached to it. Presently the test set will allow a maximum current of about 4.7×10^4 amperes to pass through it. This limit occurs because of the magnitude of the external inductance and the size of the test sets final load resistance of 0.0512 ohms. Figures 8, 9 and 10 show the current waveform for the initial load of 0.195 ohms, an intermediate value of 0.110 ohms and its final value of 0.052 ohms.

The load resistor was constructed of a strip of 80/20 Ni-Chrome material (nickel - chrome). The physical dimensions of the strips cross section are 7.87 cm x 0.043 cm (0.017 in x 3.1 in). The initial length was approximately 6.096 m (20 feet), and the initial resistance of the load was 0.197 ohms. After the third reduction in length, the final resistance was left at 0.052 ohms, and its length is 1.61m (5.3 feet).

The switching device used to transfer the energy from the thrusters capacitor bank to the test set is a triggered gap switch, Model GP-30B, manufactured by EG&G*. This switch has the capability of switching 100KA peak current pulses. The life of the switch is a strong function of the shape of the current pulse. Under preferred operating conditions, the switch can transfer a total of 5×10^3 to 20×10^3 coulombs over its useful life. The present thruster transfers 0.6 coulombs per pulse. The expected life of the switch is therefore about 8.2×10^3 to 32.9×10^3 thruster pulses. This expected life can only be obtained if the current waveform is not allowed to ring and if the pulse width does not exceed tens of microseconds. In the present design, these criteria are met. This is also one of the reasons why we have decided not to reduce the test sets load resistance below 0.052 ohms. Trimming the load resistor would allow more current to flow but would also produce a higher discharge current reversal and therefore a shorter switch life.

The switch is a three electrode device triggered from an external source. The electrical pulse which is used to fire the igniter plug of the thruster is used to trigger the

*EG&G, Salem, Massachusetts

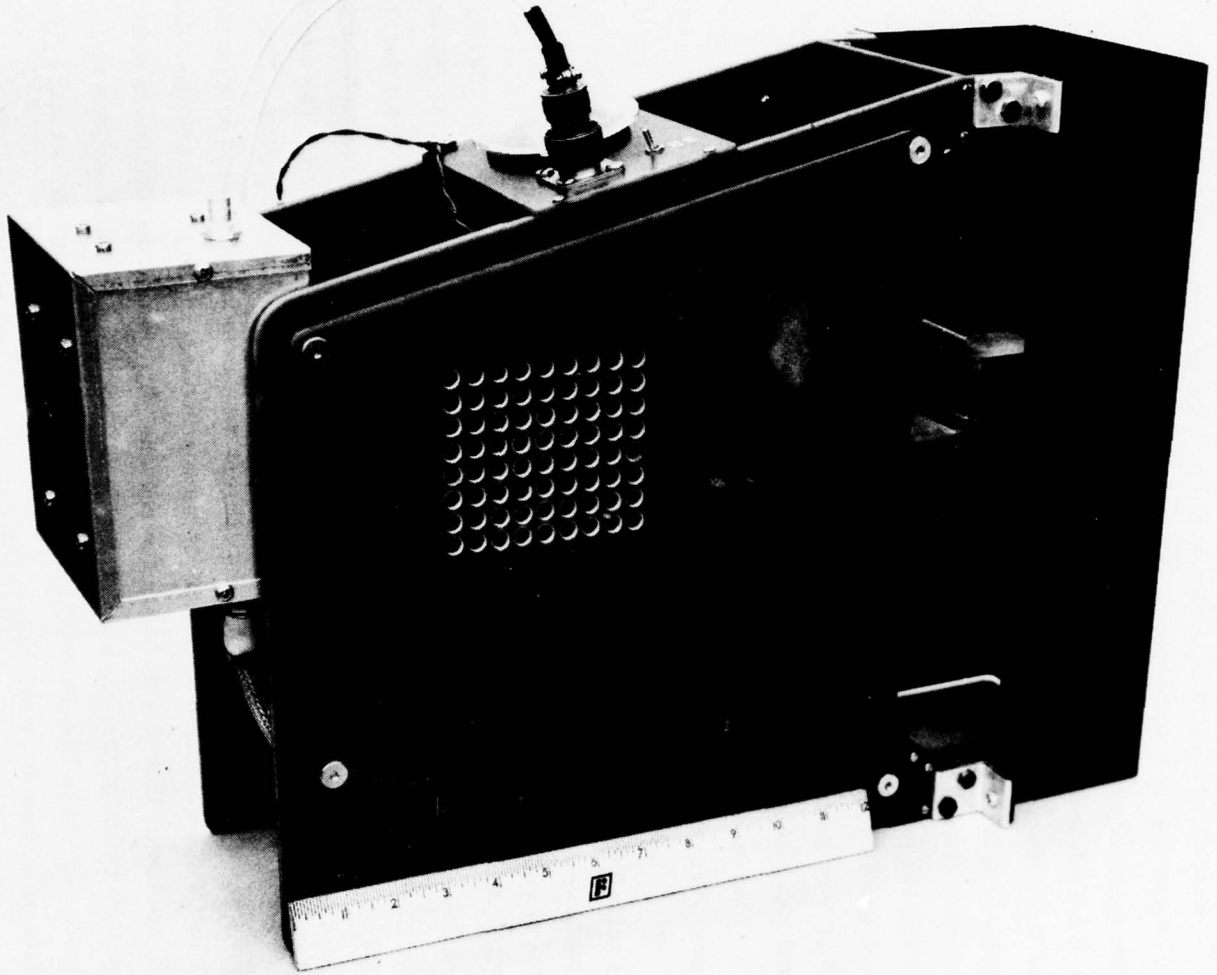

Figure 5. Thruster Test Set, Right Side

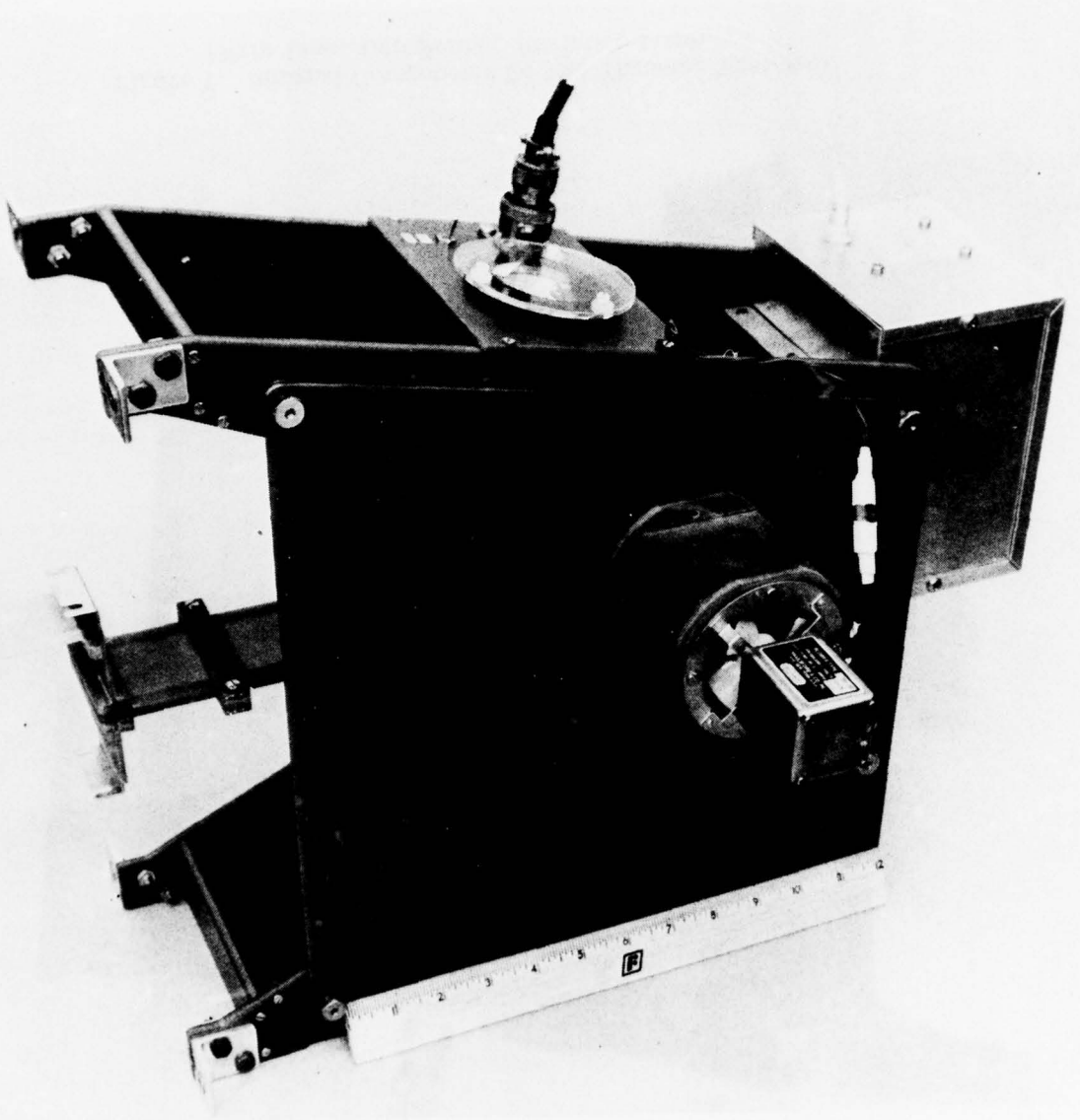

Figure 6. Thruster Test Set, Left Side

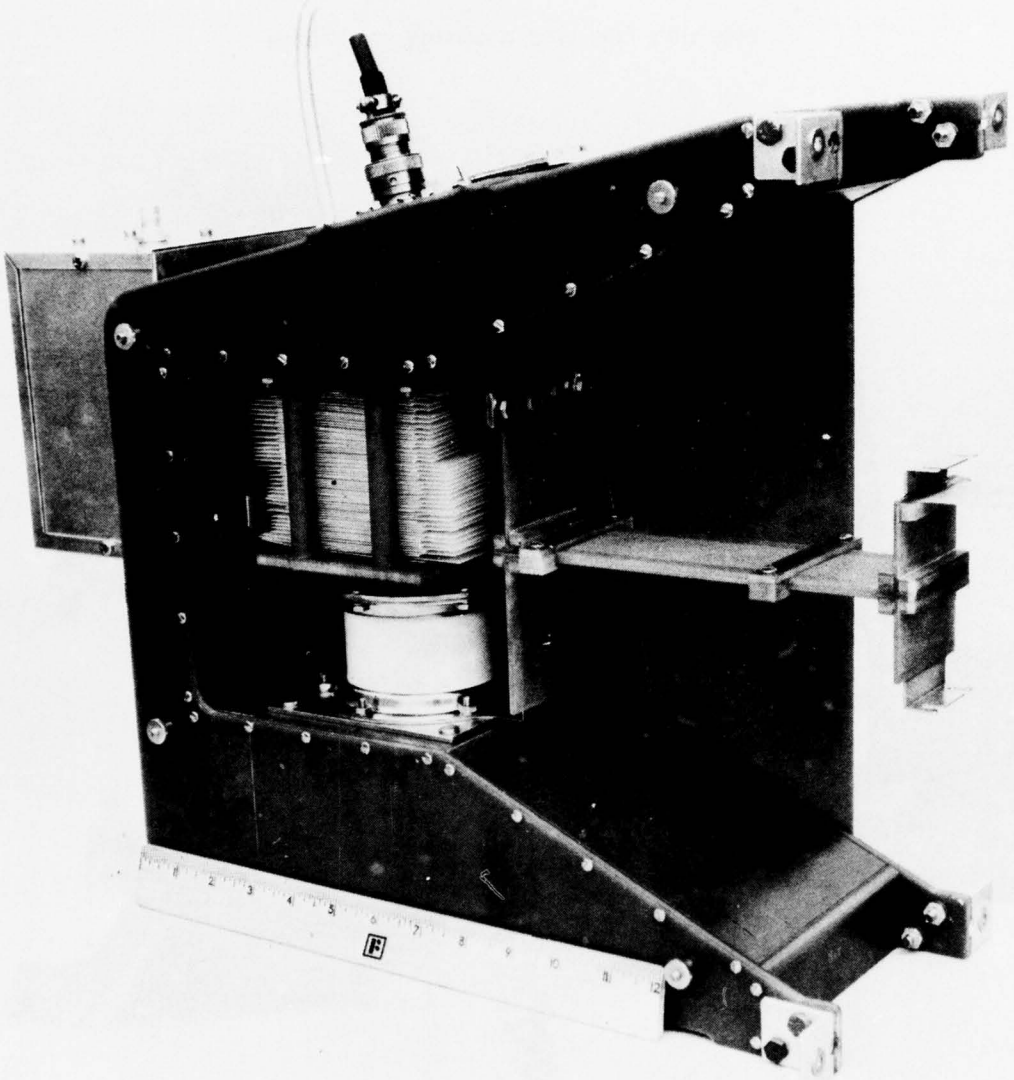

Figure 7. Internal Components Of The Thruster Test Set
(Strip Line, Gap Switch, Resistive Load)

gap switch. Figure 11 is a schematic of the triggering circuit that was developed at Fairchild Republic to trigger the switch, and Figure 12 is a schematic of the thruster capacitor bank.

The resistive load of the test set was fabricated by folding the Nichrome strip back and forth (see Figure 7). The length of each fold is approximately equal to its width. This method of folding the resistor produces a low inductance configuration. The resistive load must be capable of dissipating 150 watts of power. System operation without the resistive load produces an excessive temperature rise in the present design. For this reason, a small fan is used to keep the resistive load temperature at approximately 100° F. Figure 13 presents the number of consecutive pulses (or time) required to reach thermal equilibrium when the thruster is operated at a pulse frequency of one pulse every 7.4 sec.

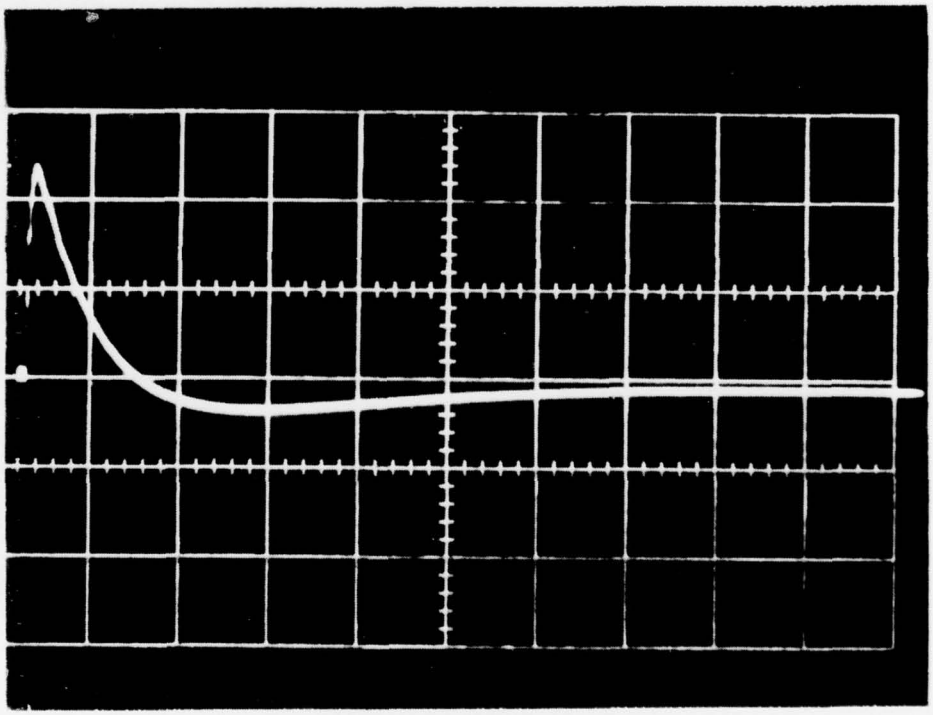

Load Resistor	0.195 ohms
Signal Amp/cm	2×10^3
Sweep speed	50 μS/cm

Figure 8. Discharge Current of One Capacitor With 0.195Ω External Load

The relevant circuit parameter for a design analysis, which is difficult to obtain, is the lumped inductance of the test set including the thruster. The other circuit parameters such as the capacitance of the thruster's bank of capacitors and the resistance of the load are readily obtained by measuring them on a bridge. We obtained an estimate of the fixed inductance of the circuit by using the current waveforms generated by an actual thruster and the waveform generated by the test set when it is connected to the thruster. Figures 15 and 16 are the waveforms that were used to calculate the inductance. Figure 15 is the

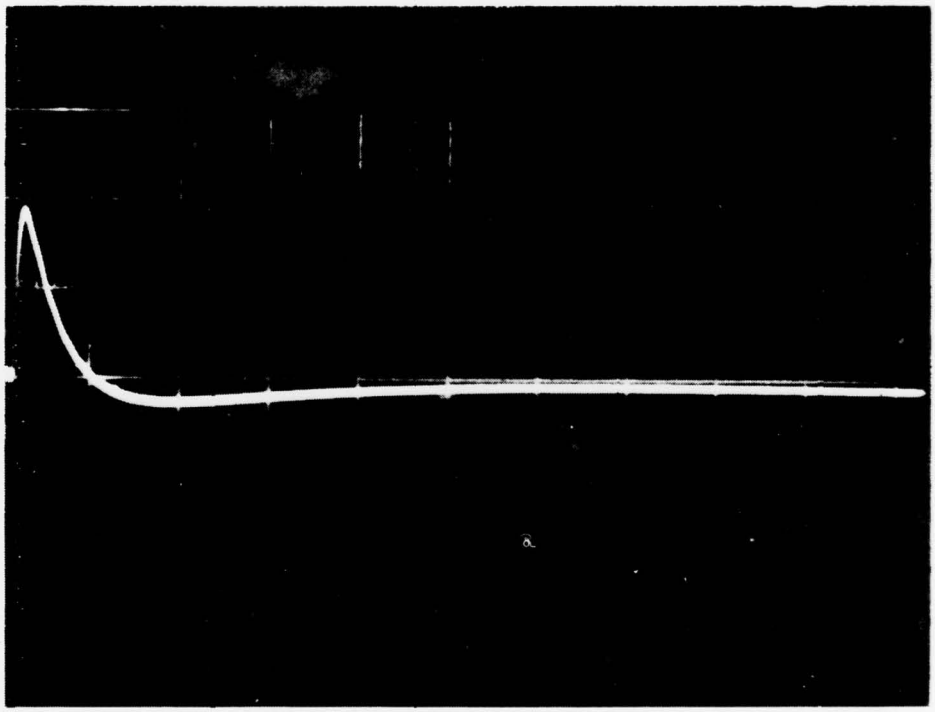

Load Resistor 0.110 ohms
Signal Amp/cm 4×10^3
Sweep Speed 50 μS/cm

Figure 9. Discharge Current of One Capacitor With 0.110 Ω External Load

waveform of an actual firing of the thruster. Figure 14 is the waveform generated with a 0.11 ohm resistive load in the test set. The inductance is calculated from the waveforms at t = 0. Using these two calculations, one can calculate the value of the external inductance and make an estimate of the total circuit inductance. The following presents a typical calculation. Assume that the circuit can be represented as shown in Figure 14.

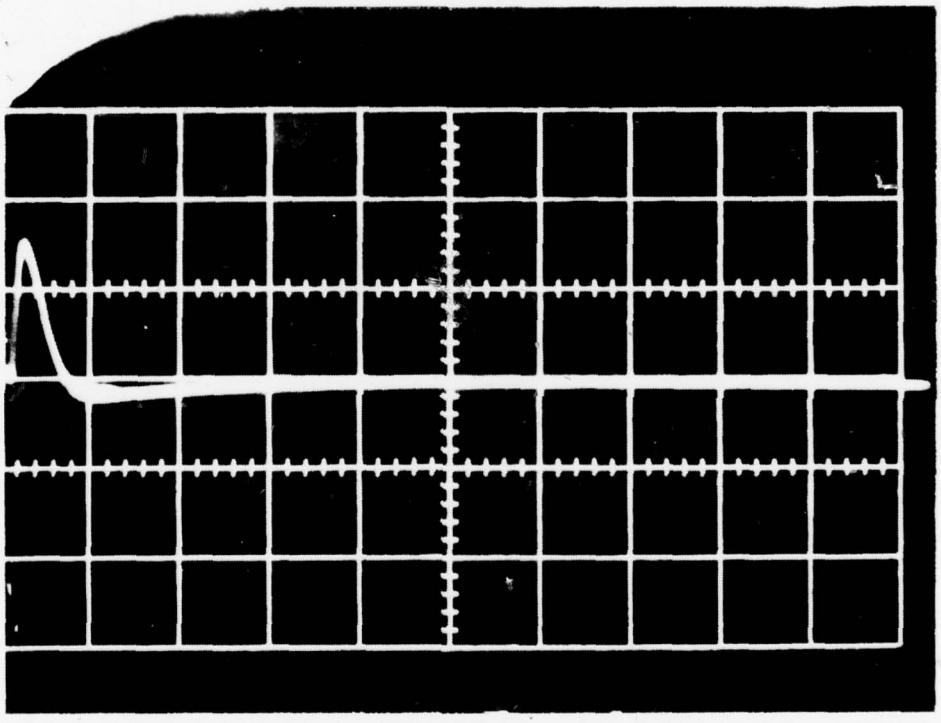

Load Resistor 0.052 ohms
Signal Amp/cm 8×10^3
Sweep Speed $50 \mu S/cm$

Figure 10. Discharge Current of One Capacitor With 0.052Ω External Load

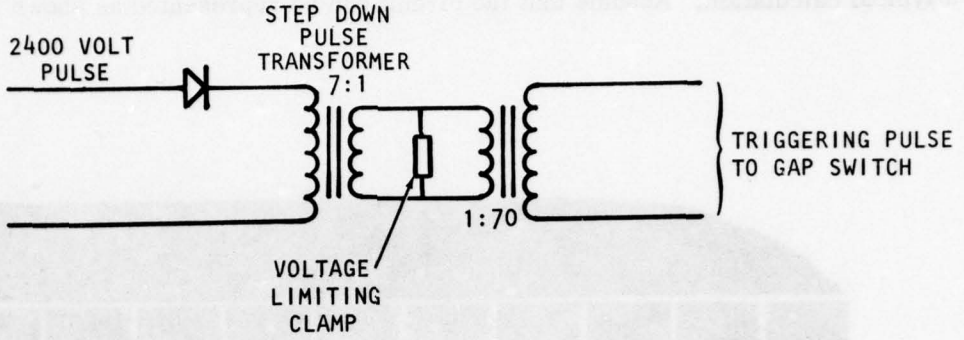

Figure 11. Gap Switch Trigger Circuit

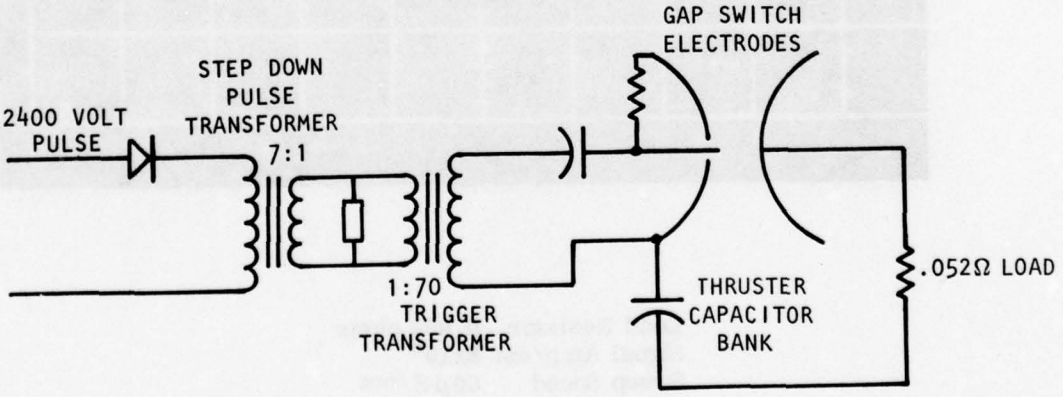

Figure 12. Schematic of Test Set Including The Thruster Capacitor Bank

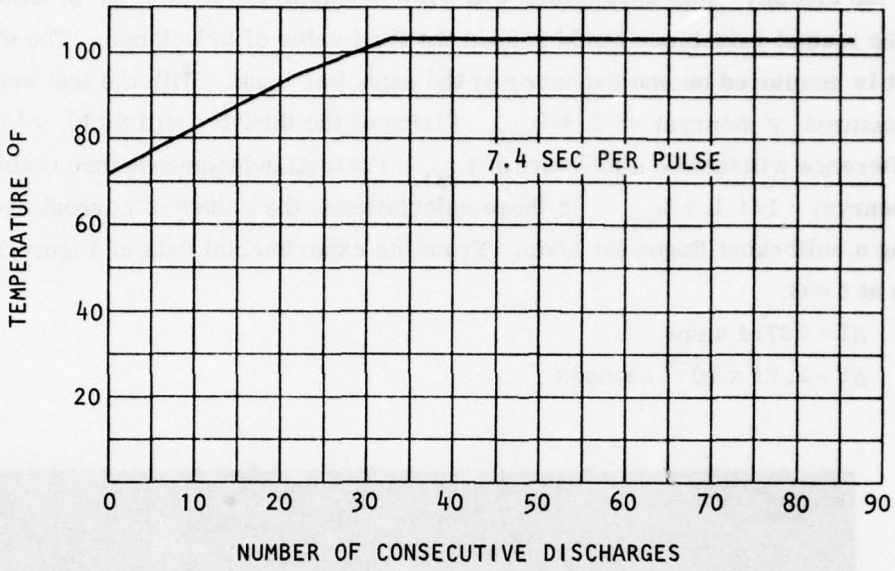

Figure 13. Temperature Variation At The Center of The Resistive Load As A Function of The Number of Consecutive Discharges

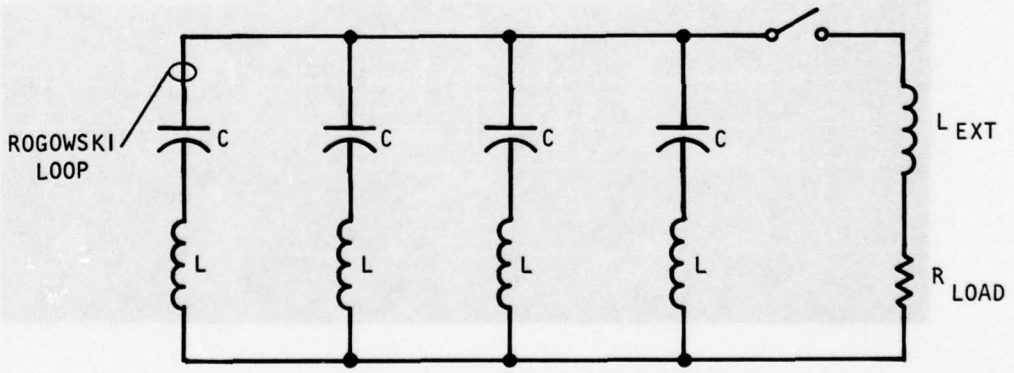

Figure 14. Schematic of Thruster Plus External Test Set Parameters

It is assumed that no interaction occurs between the circuit elements on the thruster side of the circuit. This assumption will over-estimate the final value of inductance, since the mutual inductance would reduce the final value of inductance. The discharge current is monitored on one capacitor of the capacitor bank. With the test set connected, one measures $\mathscr{L}$ (henrys) = $L + L_{ext.}$ Firing of the thruster will yield $\mathscr{L}^*$(henrys) = L. The difference will then be a measure of $L_{ext.}$ The total inductance is then estimated as $\mathscr{L}$ total (henrys) = 1/4 $L + L_{ext.}$ In these calculations, the values of current are obtained by using a calibrated Rogowski Loop. From the experimental data of Figure 15, one obtains at t = O.

$\Delta \dot{I}$ = 33714 amps

$\Delta t = 2.71 \times 10^{-6}$ seconds

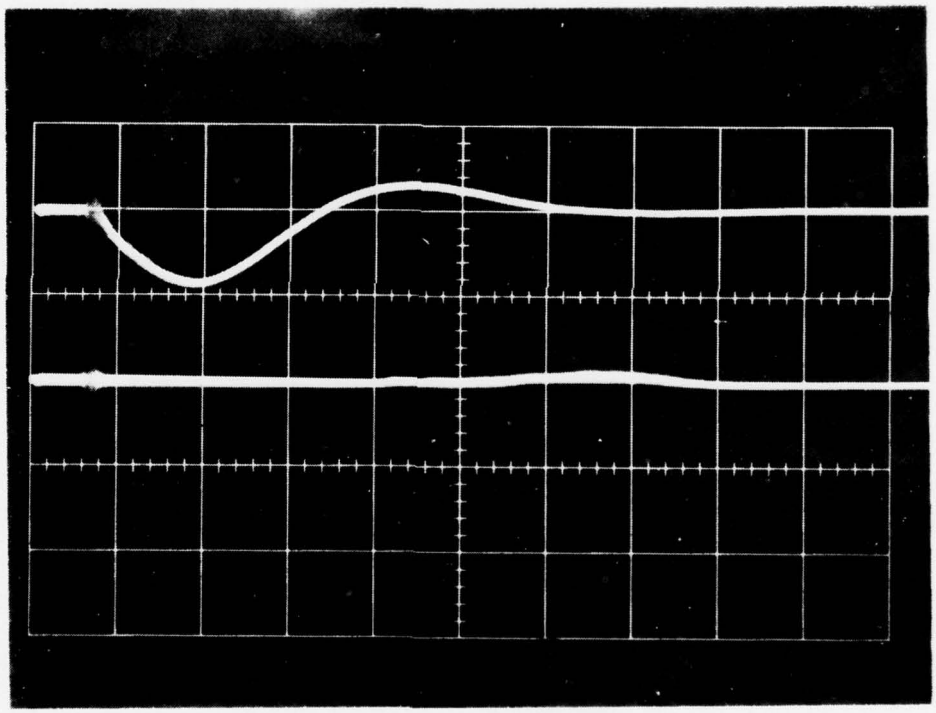

Load - Plasma
Signal 4×10^4 amps/cm
Sweep Speed 5μs/cm

Figure 15. Discharge Current of One Capacitor With Plasma As External Load

or,

$$\left|\frac{\Delta I}{\Delta t}\right|_{t=0} = \frac{Vo}{\mathscr{L}} = \frac{2414}{\mathscr{L}}$$

the value of $\left|\Delta I/\Delta t\right|_{t=0} = 1.55 \times 10^{4}$ Amps/Sec

therefore $\mathscr{L} = 1.553 \times 10^{-7}$ henrys

Similarly, one finds from Figure 16 that $\mathscr{L}^{*} = 8.457 \times 10^{-7}$ henrys. The value of L_{ext} is therefore 6.904×10^{-7} henrys.

The total inductance is then estimated as $L_{total} = 1/4\ (1.553 \times 10^{-7}) + 6.904 \times 10^{-7}$

$= 7.292 \times 10^{-7}$ henrys.

Figure 15 was obtained with a thruster whose capacitor bank was slightly larger than the present thruster. This is evidenced by the voltage which is used for a 750 joule discharge. This means that the two thrusters have the same inductance within a few percent.

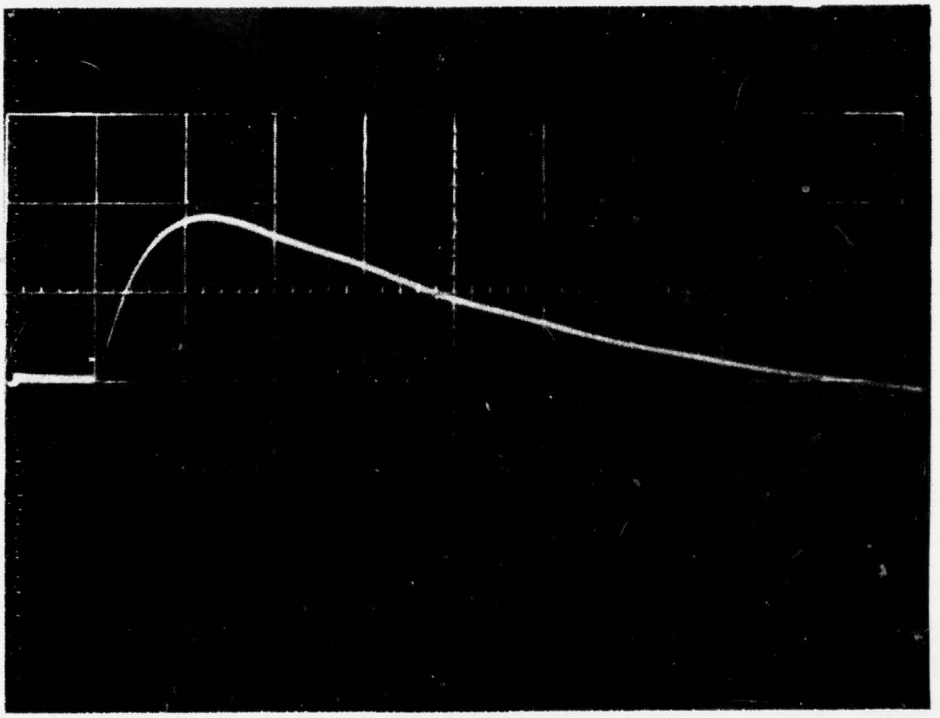

Load Resistor (.110Ω)
Signal 4×10^{3} amps/cm
Sweep Speed 5μs/cm

Figure 16. Discharge Current of One Capacitor with 0.110 Ω External Load

The peak discharge currents were calculated from the photographs and also from the expression for the peak current in an oscillatory discharge:

where

$$I_p = V_o \sqrt{C/L}\ e^{-\alpha t_p}$$

I_p = peak current (amperes)

Vo = Voltage on the capacitor bank

C = Capacitance of the bank

α = R/2L

t_p = time to reach maximum current. This value is taken from the photograph.

For R = 0.110 ohms, the value of peak current from Figure 15 is 2.89×10^3 amps. The value obtained from the above analytic expression is 2.84×10^3 amps. The two results agree quite well with each other. If we recalculate the circuit inductance for R = 0.052 ohms, we find that the inductance value is 7.275×10^{-7} henrys. The calculated current on this basis is 3.55×10^4 amperes. The peak current as measured from the oscilloscope is 4.7×10^4 amperes. The reason for this discrepancy is due to the effect of the true value of inductance. As mentioned above, the estimate of the inductance assumed no interaction. This assumption leads to a higher value of inductance. A better estimate of the inductance would have been obtained if we had measured the current flowing between the load and the thruster. Under these circumstances, we would have measured the total current flow and the equivalent circuit inductance for the configuration of interest. At the time these measurements were being made, we had only one calibrated Rogowski coil, and it was mounted on one of the capacitors in the thruster. In any event, if we assume that the damping factor assumes the smallest value, we would have to have an inductance of 6.495×10^{-7} henrys. Thus our true inductance for the system is bounded by $7.275 \times 10^{-7} > L_{true} > 6.495 \times 10^{-7}$ henrys for a resistive load, R, of 0.052 ohms.

The unshielded test set in its present configuration provides a current pulse of about 47 kilo-amps when used with the thruster. Presently a fan is necessary to keep the resistor test load from overheating. The load temperature rises to 102° F under steady running conditions of 1 pulse every 7.4 seconds. To simplify integrating a thruster to a spacecraft, it would be advantageous if the test set was used with the thruster also under vacuum conditions. From a materials point of view, the test set components are/or can easily be made completely compatible with the vacuum - temperature environment. The only design problem that would have to be resolved is the technique of dissipating the heat

generated in the resistive test load under vacuum conditions. Two approaches can be suggested for keeping the test load from overheating in a vacuum:

1) Radiative cooling
2) Thermal conduction to a heat sink

If we assume radiative cooling as the only mechanism for controlling the resistive load temperature, then we can expect a radiator whose effective radiation area is approximately 0.6 m^2. This estimate assumes a vacuum chamber wall temperature of 50°C (worst case), and a radiator temperature of 100°C. This is based on the maximum operating temperature of the gap switch which is 100°C. The emissivities are assumed to be 1, and the geometric factor is taken to 0.5. In the second case of conductive cooling, many methods are available, but the final choice would depend on the immediate application and test conditions.

4.0 EMI TESTS

4.1 Unshielded Test Set Noise and Shielding Effectiveness Test

Testing of the unshielded test set for its electromagnetic noise, as well as the shielding effectiveness tests of the thruster enclosure were carried out in a shielded room at the test laboratories of Dayton T. Brown in Bohemia, N.Y..

The item to be evaluated was set up within a shielded room acting as an enclosure which is 20 feet wide by 20 feet long by 10 feet high. All lines carrying power into the shielded room passed through RF suppression filters suitably bonded to the enclosure and capable of 100 dB attenuation over a spectrum of 14 kHz to 10,000 MHz. All neutral lines entering the enclosure were bonded to the same point of entry.

Bonding of the item to be tested was achieved by means of ground straps soldered to the ground plane. The DC bond impedance, from the item being tested to the ground plane, was less than 2.5 milliohms. All antenna during radiated emission and susceptibility testing were located at least 1 meter from all walls of the shielded enclosure.

For interference measurements, the "Broadband...Peak Detector, Wide Bandwidth" receiver function was utilized.

4.1.1 Unshielded Test Set Noise Test

The noise generated by the unshielded test set when pulsed was measured at three locations. The three positions are as follows:

1) One meter to the right (designated the "rear") of the small aluminum box on the right side of the test set as shown in Figure 1 of this report.
2) One meter to the left of the thruster enclosure (designated "front") as shown in Figure 1.

3) One meter from the side of the thruster enclosure shown in Figure 1 (designated "side").

The electromagnetic noise spectrum and the field quantity measured are shown in Table 1.

TABLE 1. SPECTRUM AND MEASURED FIELD QUANTITY

Frequency	Electric Field	Magnetic Field
15 KHz	X	X
30"	X	X
60"	X	X
120"	X	X
250"	X	X
500"	X	X
1 MHz	X	X
2 MHz	X	X
4 MHz	X	X
8 MHz	X	X
16 MHz	X	X
25 MHz	X	X
50 MHz	X	-
100 MHz	X	-
200 MHz	X	-
400 MHz	X	-
800 MHz	X	-
1000 MHz	X	-
1600 MHz	X	-
3200 MHz	X	-
6400 MHz	X	-
10,000 MHz	X	-

Table 2 presents a list of the test equipment that was used for the noise measurements.

TABLE 2. LIST OF EQUIPMENT USED FOR NOISE TEST

Item	Manufacturer	Equipment Characteristics	Accuracy	Model	Cal.
1) Spectrum Surveillance System	Fairchild	0 Hz to 1 GHz	Mfr's data available	FSS-250	6 months
2) Interference Analyzer	Fairchild	14 KHz to 1 GHz	Mfr's data available	EM e-25	6 months
3) Rod Antenna	Fairchild	14 KHz to 30 MHz		RVR-41	6 months
4) Biconical Antenna	White Electro-magnetics	20 MHz to 200 MHz	Maint. only	407A	2 years
5) Log Spiral Antenna	Electro-Mechanics	100 MHz to 2 GHz	Mfr's data available	3101	2 years
6) Log Spiral Antenna	Electro-Mechanics	1 GHz to 10 GHz	Mfr's data available	CLP-1B	2 years
7) Loop Antenna	Fairchild	10 KHz to 25 MHz	Mfr's data available	ARL-25	2 years
8) Screen Room	Ace Engineering & Machine Co.	14 KHz to 10 GHz	-	20'x20'x10'	-
9) Spectrum Analyzer	AIL Tech.	2 MHz to 20 GHz	Mfr's data available	727	6 months

Radiated emissions of the magnetic field were measured over a frequency spectrum from 0.015 to 25 MHz with a loop antenna. The antenna was located 1 meter from the test sample. Location of the antenna with respect to the test sample was ascertained on the basis of probing the sample. The antenna per meter factors of the antenna utilized are known and recorded.

Radiated emissions of the electric field were measured over a frequency spectrum from 0.015 to 10,000 MHz. The following applicable antennas were employed:

Spectrum (MHz)	Antenna
0.014 to 25	41 Inch Rod
25 to 200	Biconical
200 to 1000	Conical Log Spiral
1000 to 10,000	Conical Log Spiral

All antennas were located 1 meter from the test sample. Location of antennas with respect to the test sample was ascertained on the basis of probing the sample. In the frequency range of 25 to 200 MHz, both horizontal and vertical components of radiated emissions were measured. The antenna per meter factors of all antennas utilized are known and recorded.

Figures 17 through 20 present the experimental setups with the three different locations of the antennas for the electrical tests as well as the loop antenna for the magnetic field tests, respectively.

The magnetic field measurements were made from 15 KHz to 25 MHz. This range is based on para. 5.1.2.1.4 of MIL-STD-1541. The REO2 electric field measurements of the same document were based on para. 5.1.2.2.3 with the upper limit at 10 GHz. Unfortunately, the upper frequency bands of the analyzer of D.T. Brown were noisy. This problem precluded the observation of generated noise at 3.2, 6.4 and 10 GHz. It can be said, however, that the noise from the test set is less than the level indicated at the above frequencies. Despite the presence of the receiver noise, one set of data is presented out to 10 GHz to show the level of equipment noise. All other graphs of the electric field noise would show the same limiting receiver noise data at 3.2, 6.4 and 10 GHz.

Prior to full testing, a preliminary survey was undertaken from 15 KHz to 1 GHz to determine attenuation ranges for proper receiver operation. Statistics were also taken to determine the number of thruster pulses required to obtain a maximum signal intensity. At frequencies less than 2 MHz, there were only small variations in signal intensity from pulse to pulse. These small variations were due to the fact that the fields are generated by the arc current which is fairly constant on a pulse to pulse basis. At the higher frequencies, the Fourier components of the current pulse are attenuated. At the higher frequencies, we begin to see statistical variation in the data. For example, the variation in the magnetic field data noted at 25 MHz on a ten shot basis was 6 db between the minimum signal and the maximum signal. Data was also taken on a 25 shot basis. The variation in the maximum to minimum signal as compared to a ten shot sequence was 1 to 2 dB. It was concluded that 10 consecutive thruster pulses would be adequate to determine the maximum signal within 2 dB. It should be noted, however, that the cited statistical magnetic field variation of 6 dB at 25 MHz is not the maximum variation noted at other frequencies. The statistical variation as a function of frequency is presented along with the general data.

Polarization of the noise from the unshielded test set was also checked. This check was done from 25 MHz to 200 MHz using the biconical antenna. There was no significant difference between the vertical and horizontal electric field.

Figures 21, 22 and 23 present the measured electric field emission of the unshielded test set as a function of frequency (up to 1 GHz) in front, to the side and to the rear of the thruster/test set, respectively. The statistical variation on 10 consecutive pulses is

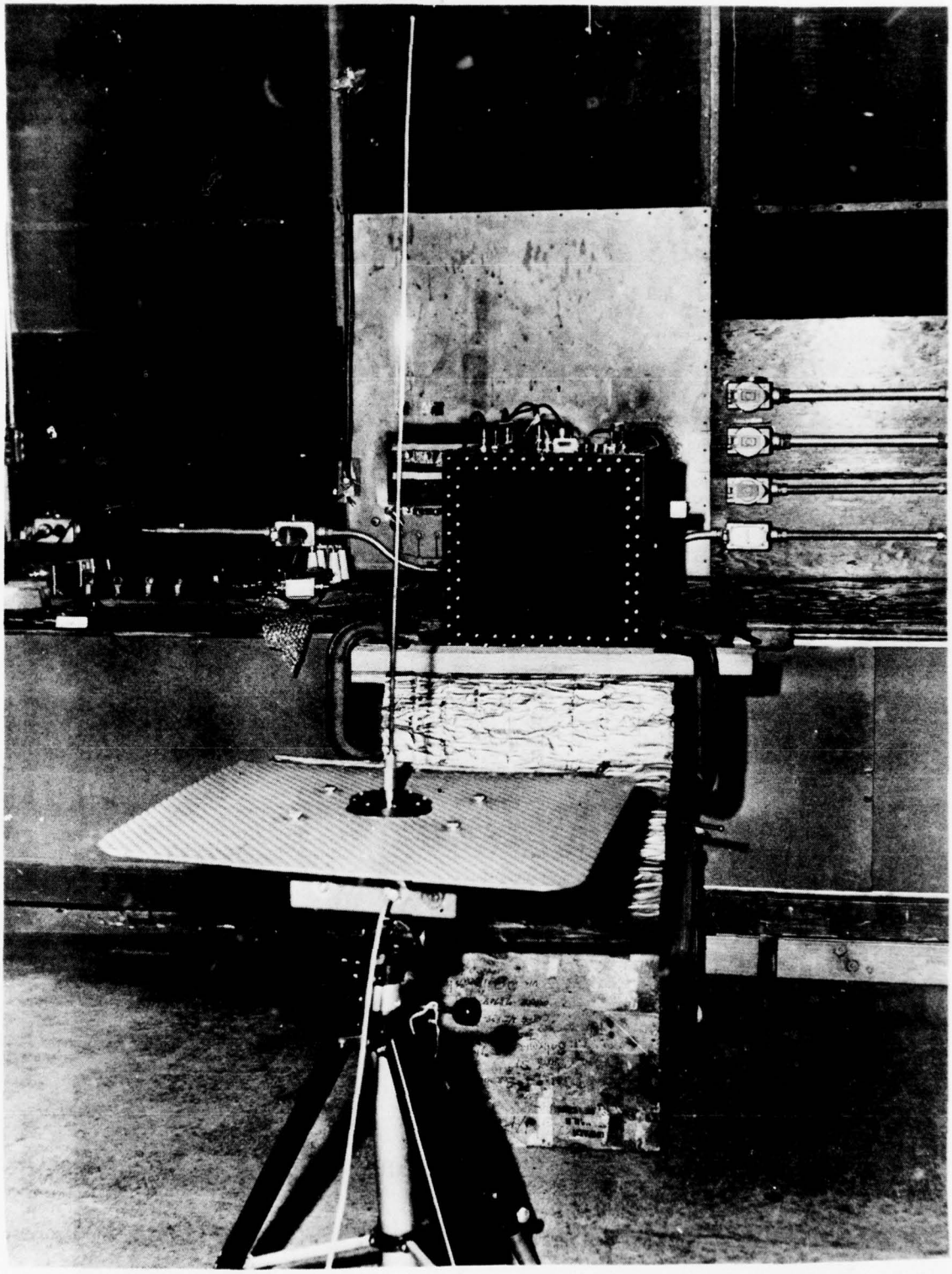

Figure 17. Laboratory Set Up (Front) For Electric Field Noise Emissions Measurement Using RVR-41' Rod Antenna (14 KHz - 27 MHz)

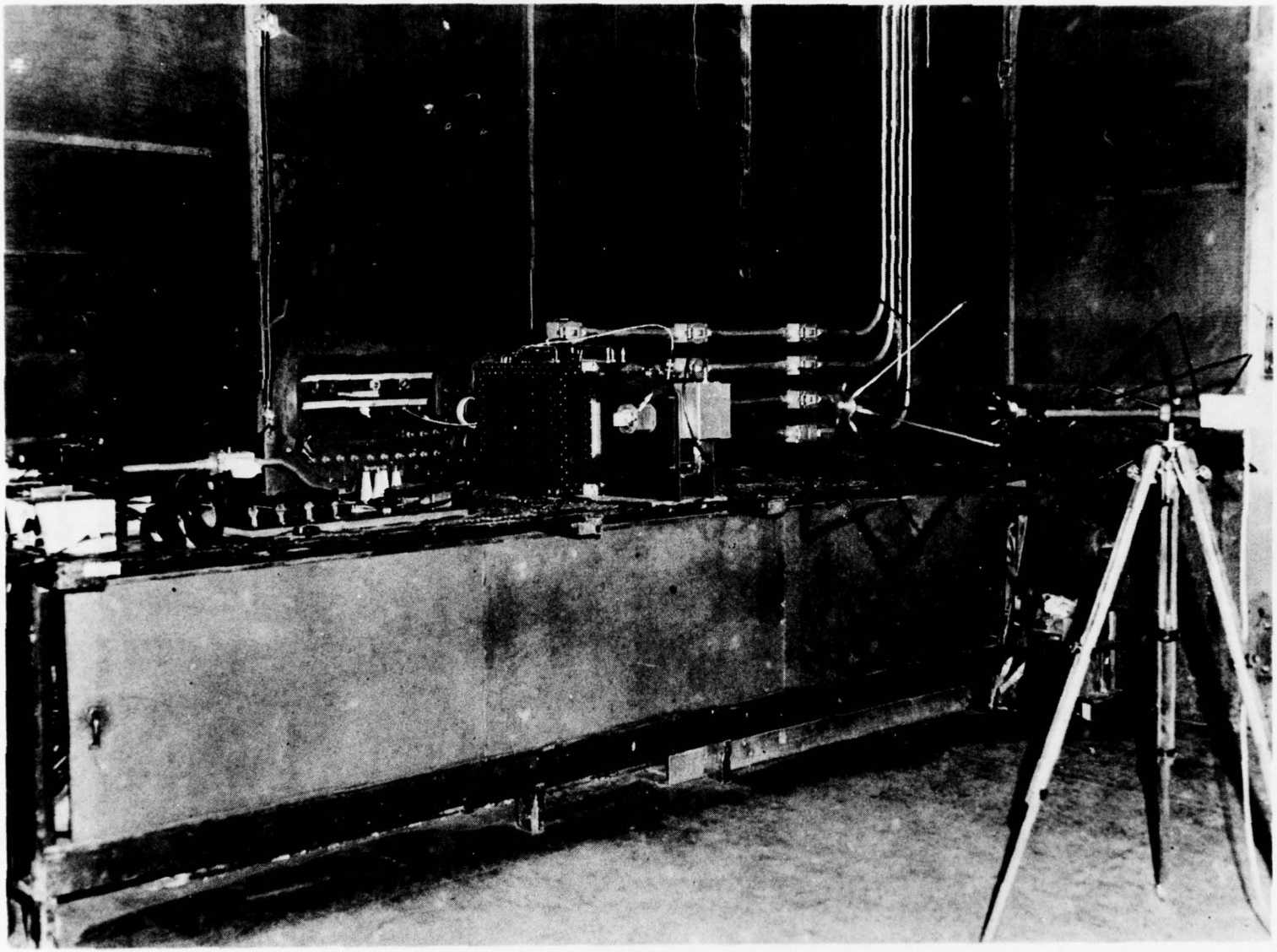

Figure 18. Laboratory Set Up (Rear) For Electric Field Noise Emission Measurement Using Bi-Conical Antenna (20 - 200 MHz)

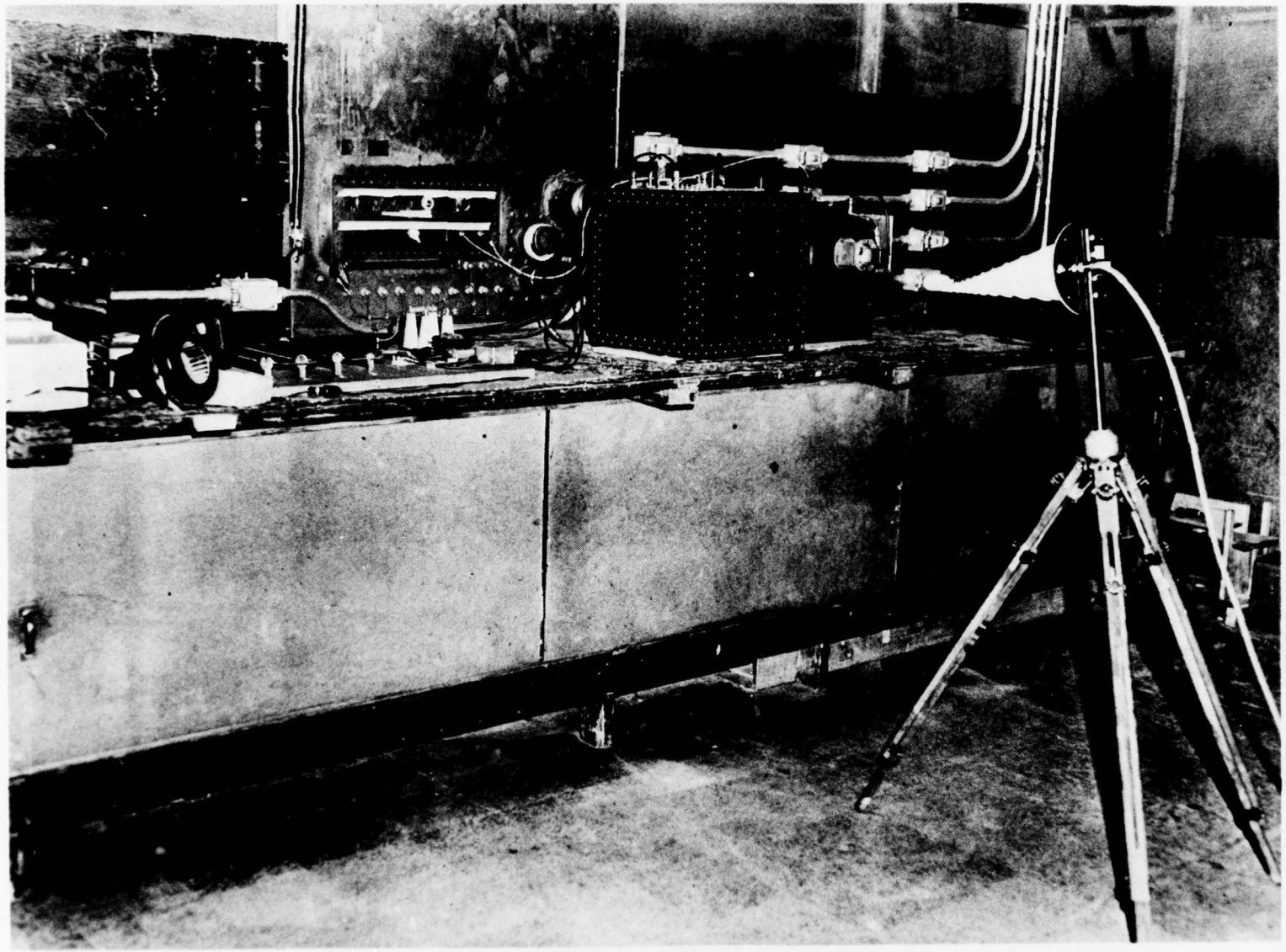

Figure 19. Laboratory Set Up (Left Side) For Electric Field Noise Emissions Measurement Using Conical Log Spiral (1 - 10 GHz)

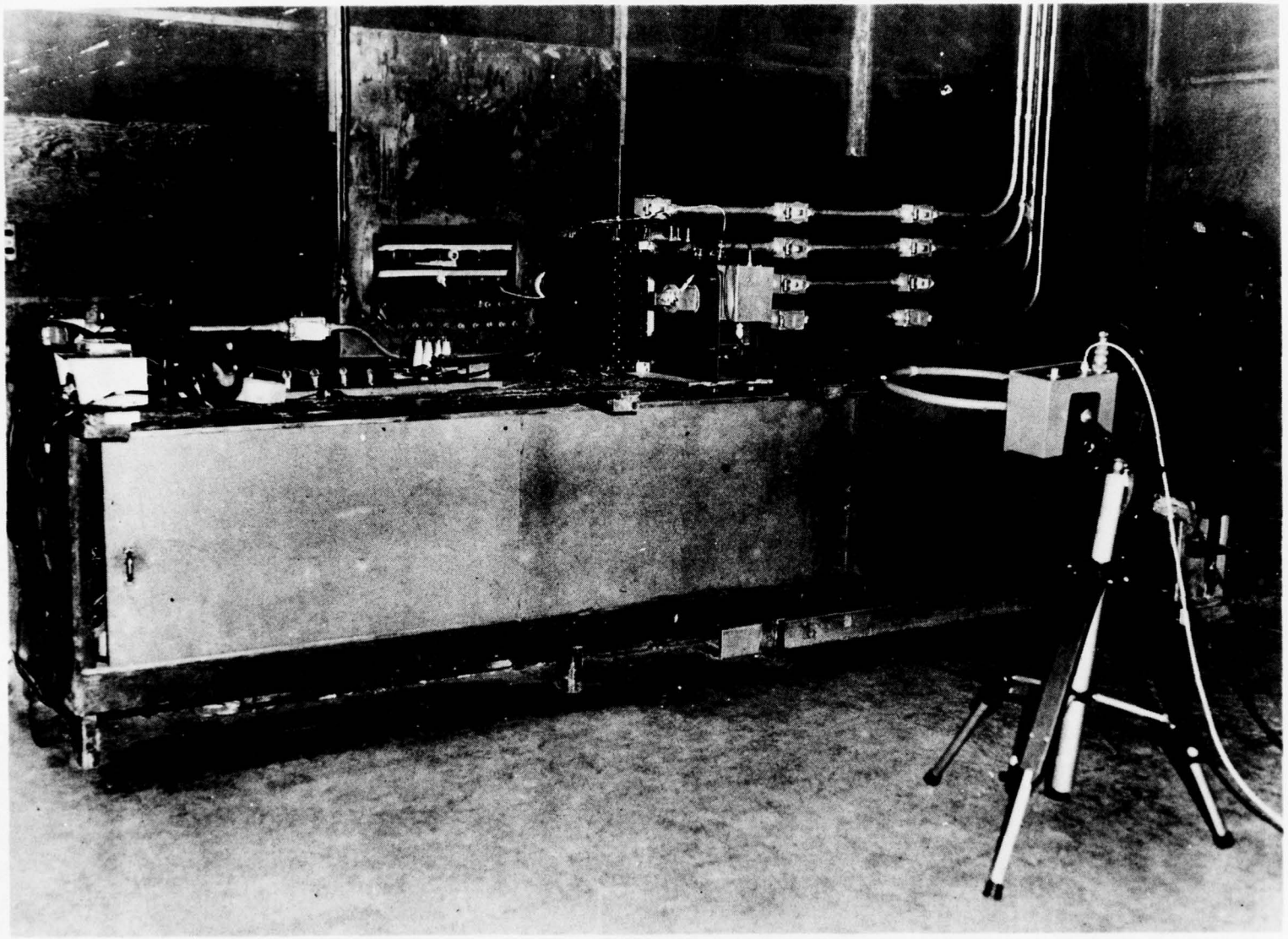

Figure 20. Laboratory Set Up For Magnetic Field Noise Emissions Measurement Using Magnetic Loop (15 KHz - 30 MHz)

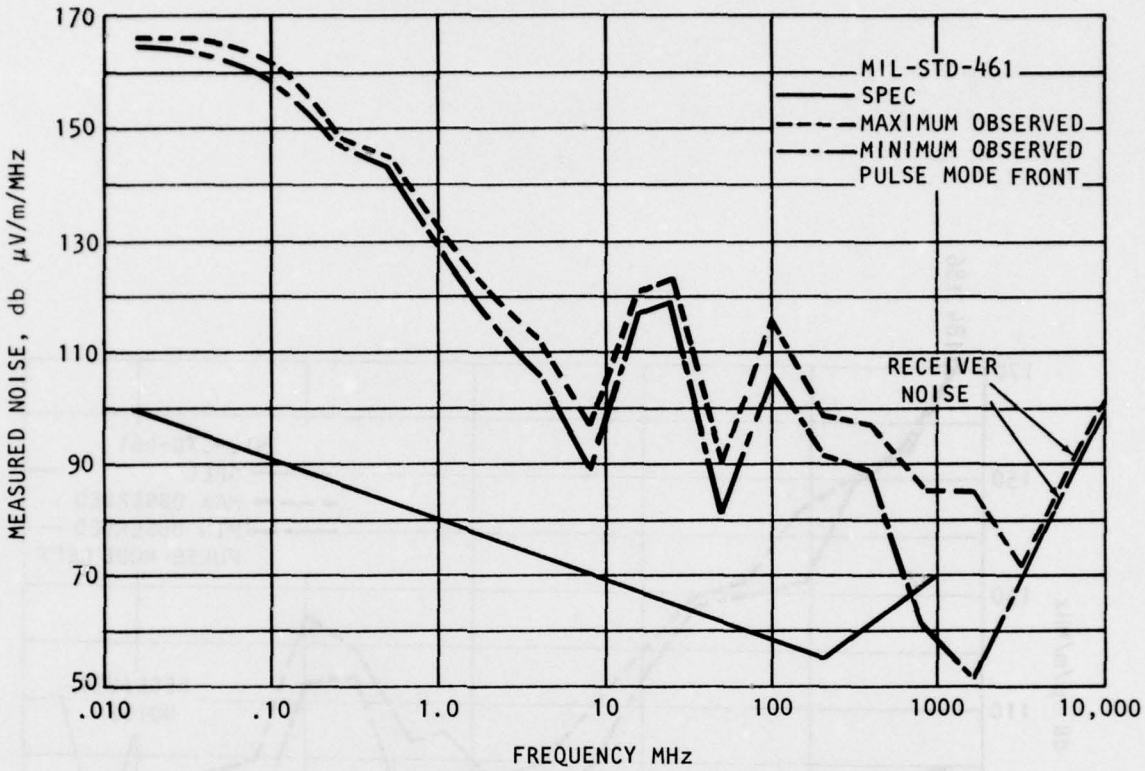

Figure 21. Radiated Electric Field Emissions
(15 KHz - 10 GHz, Front)

presented in the format of two data lines. The requirements of MIL-STD-461A and 1541 are also included for comparison. Figure 24, 25 and 26 present the measured magnetic field emissions by the unshielded test set in front, to the side and to the rear of the thruster/test set, respectively. The electric field emission of the unshielded spark gap trigger at the rear of the thruster/test set is presented as Figure 27. The corresponding magnetic field emission is presented as Figure 28. The noise radiated by the cooling fan of the test set was observed over the range 15 KHz to 250 KHz. This noise was of a lower level and can be easily shielded.

4.1.2 Discussion of Unshielded Test Set Noise Data

The data of the unshielded test set presented in Section 4.1.1 indicated the presence of a broad based noise signal which, as expected, is generally outside MIL-STD-1541 and 461. The lower frequency end of the measured spectrum indicated a relatively constant

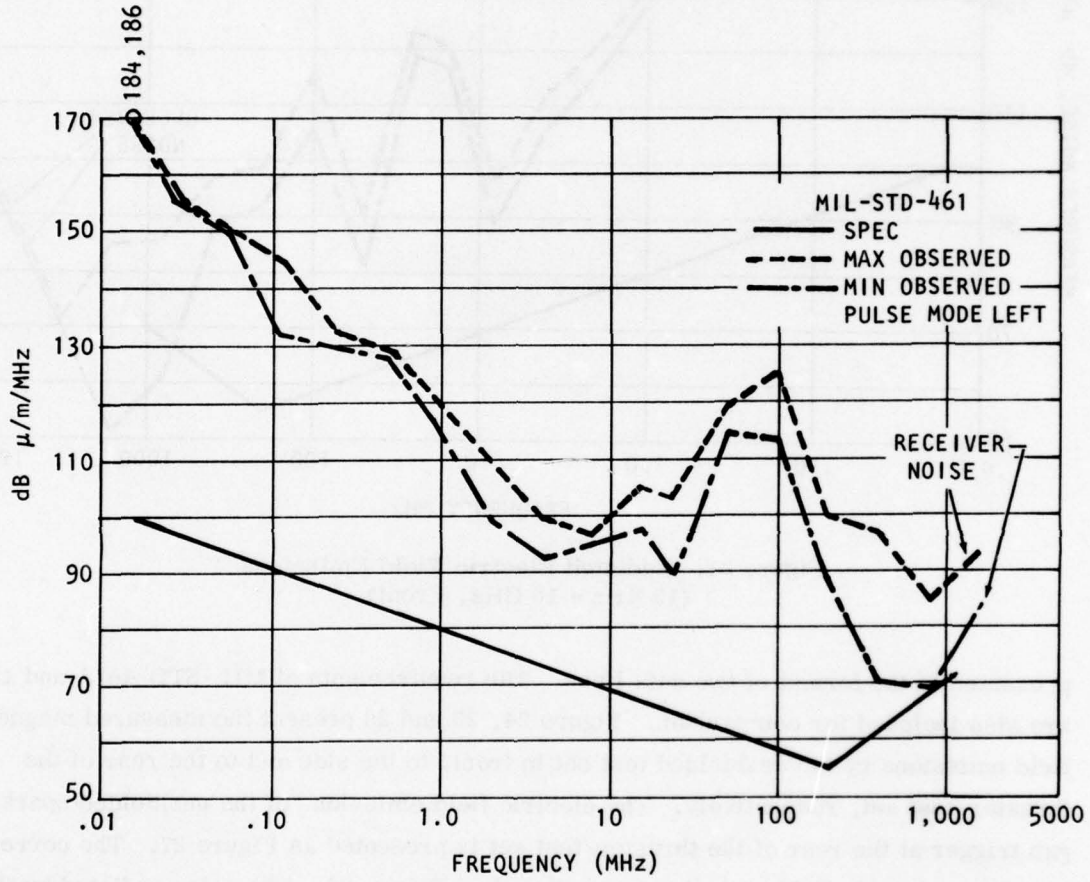

Figure 22. Radiated Electric Field Emissions (15 KHz - 16 GHz, Left Side)

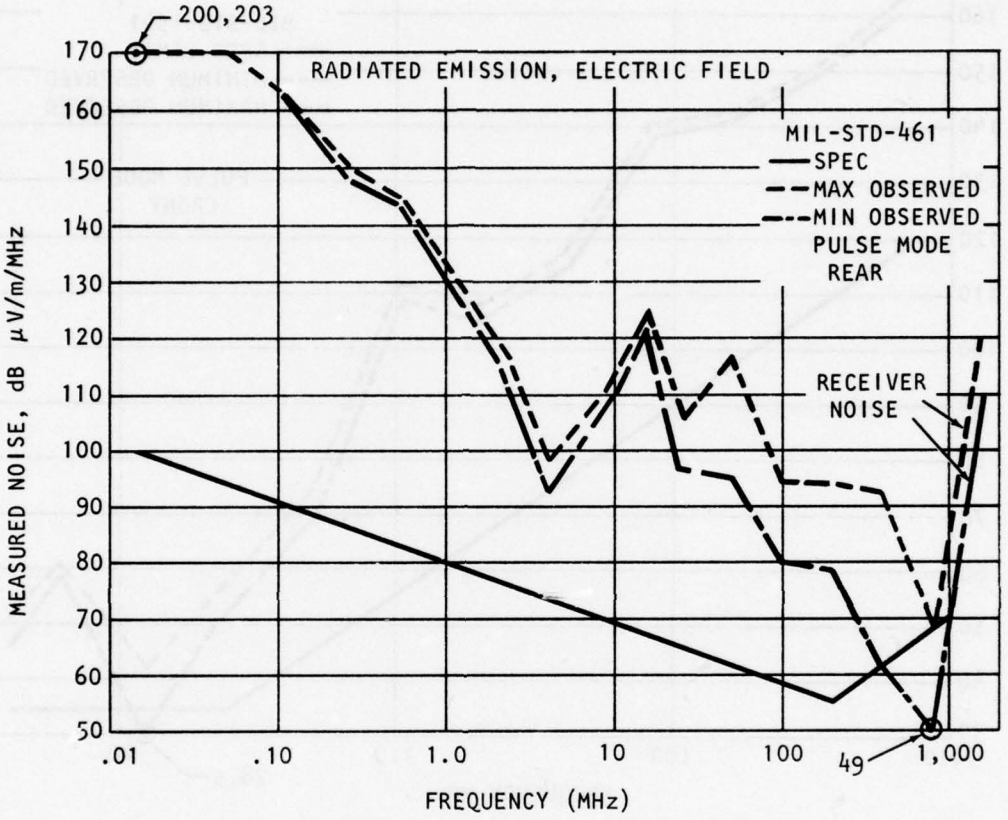

Figure 23. Radiated Electric Field Emissions (15 KHz - 1.6 GHz, Rear)

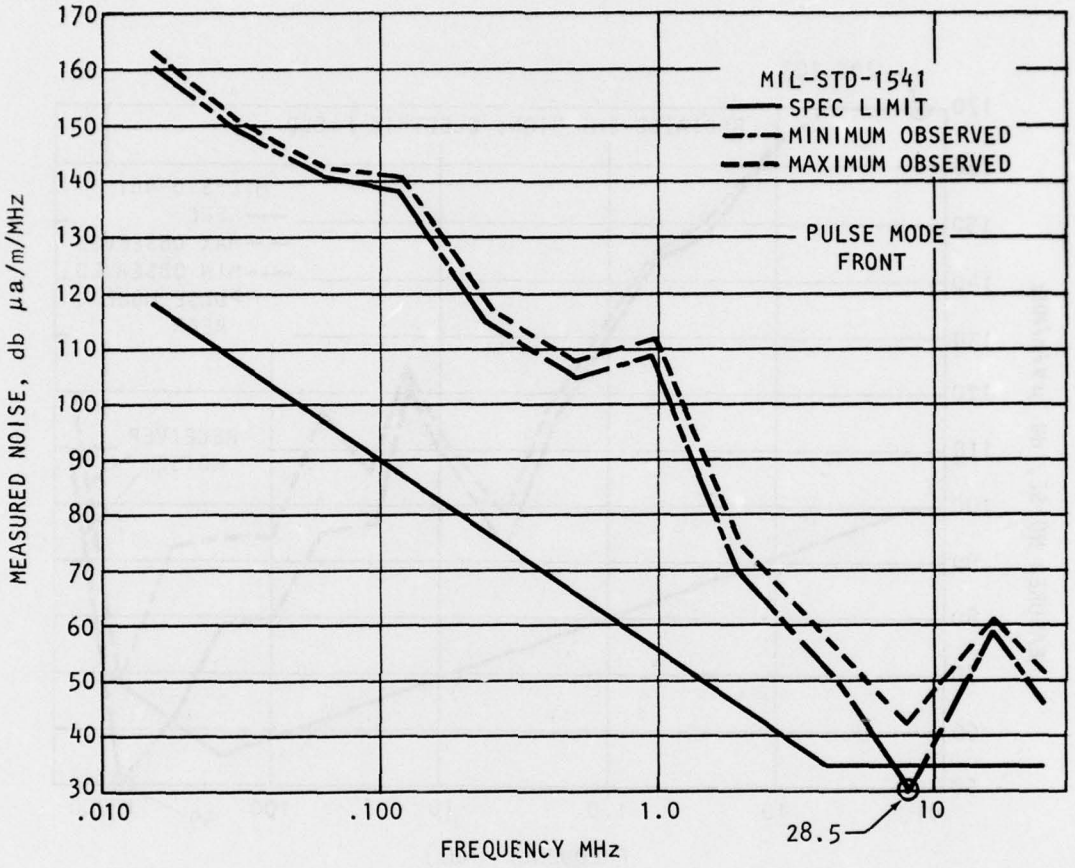

Figure 24. Radiated Magnetic Field Emissions
(15 KHz - 25 MHz, Front)

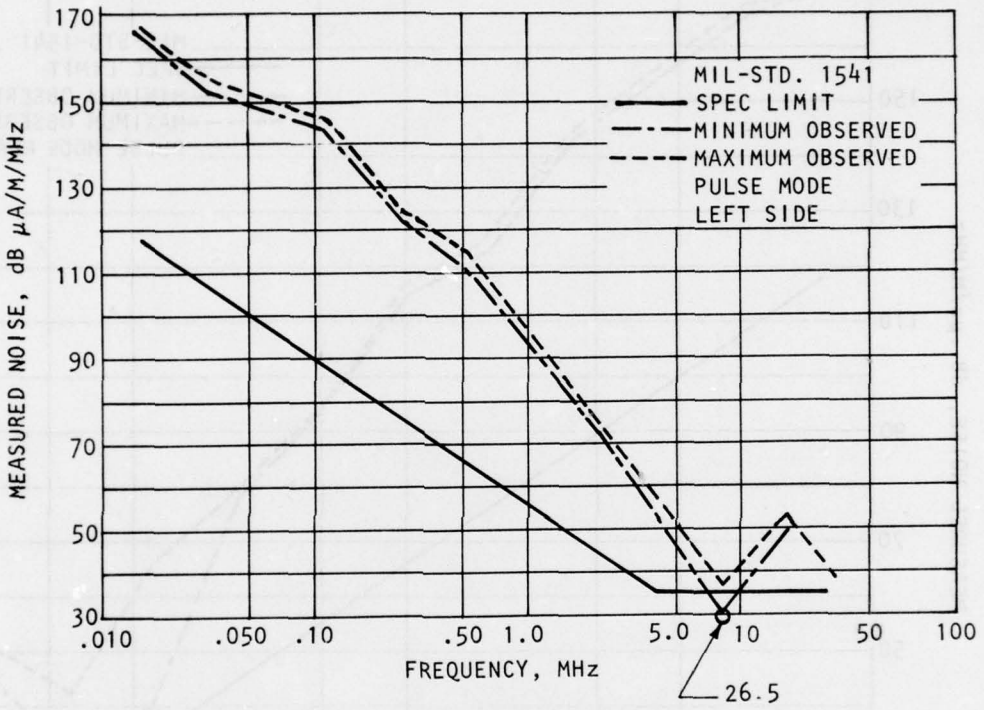

Figure 25. Radiated Magnetic Field Emissions
(15 KHz - 25 MHz, Left Side)

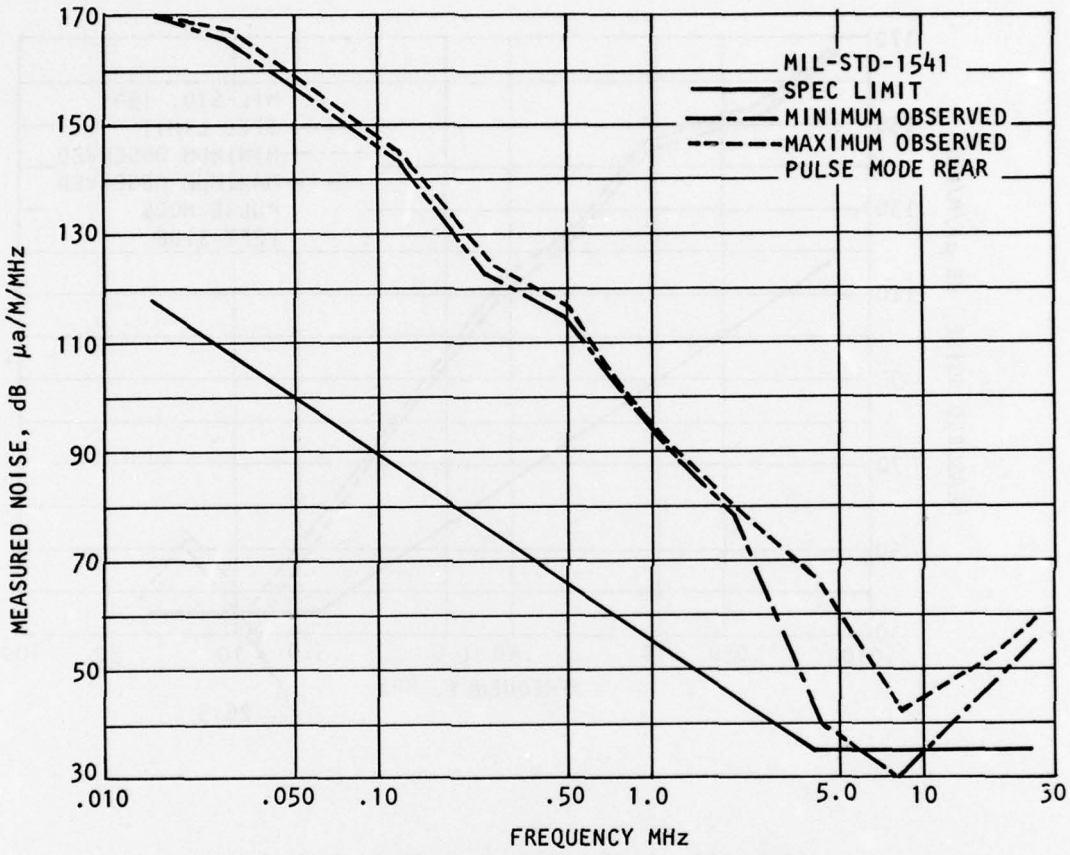

Figure 26. Radiated Magnetic Field Emissions (15 KHz - 30 MHz, Rear)

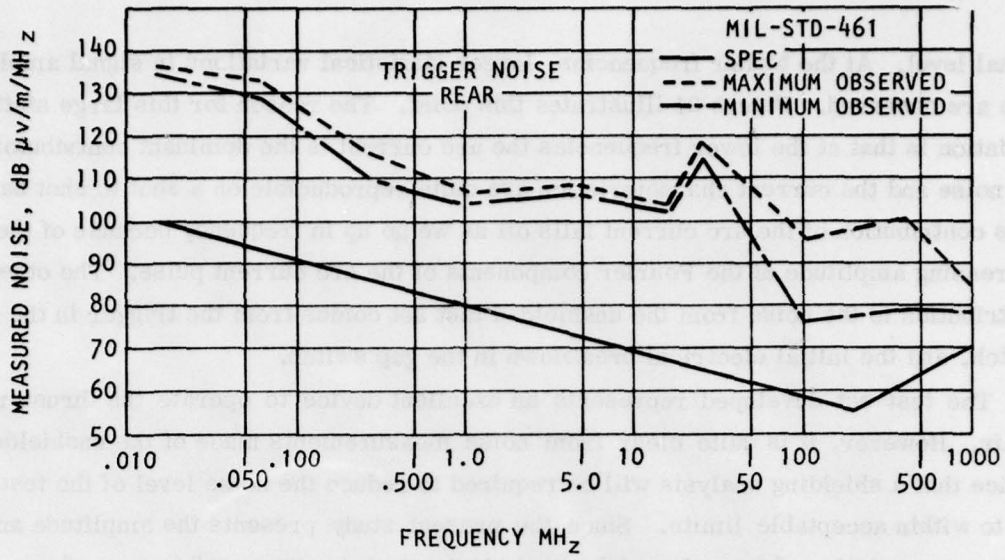

Figure 27. Radiated Electric Field Emissions (15 KHz - 1 GHz, Trigger Noise, Rear)

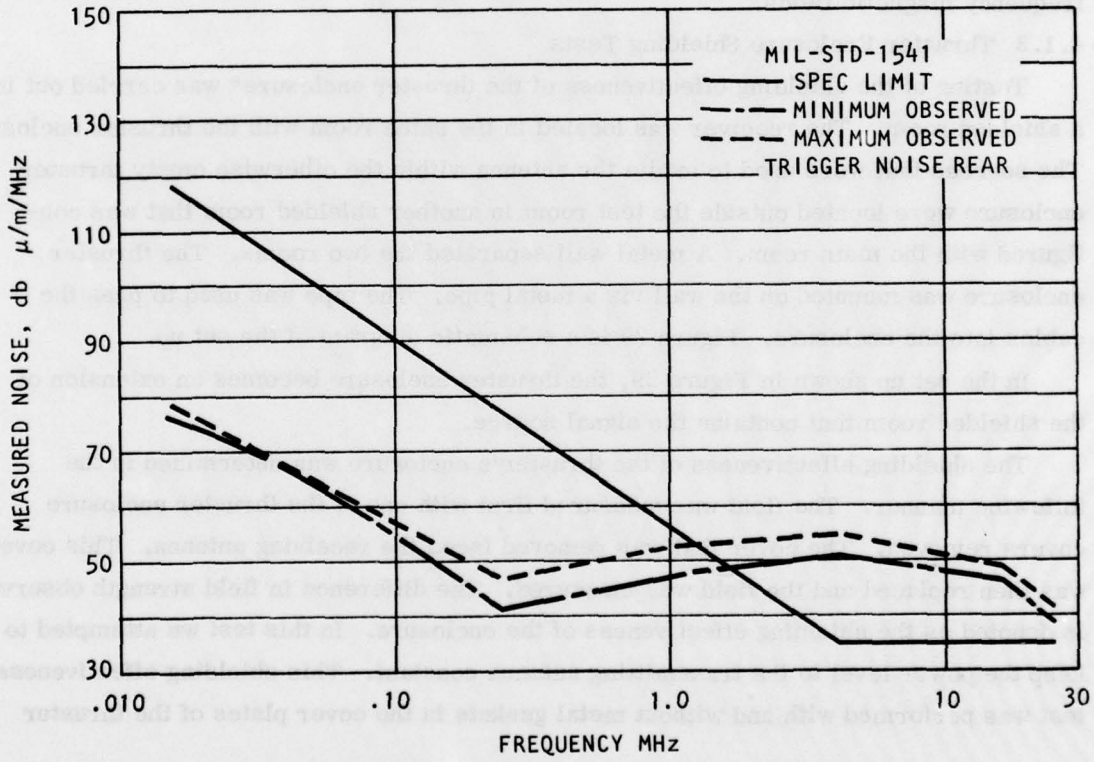

Figure 28. Radiated Magnetic Field Emission (15 KHz - 30 MHz, Trigger Noise, Rear)

signal level. At the higher frequencies, larger statistical variations in signal amplitude are observed. Figure 21 illustrates this point. The reason for this large statistical variation is that at the lower frequencies the arc current is the dominant contributor to the noise and the current characteristics are quite reproducible on a shot to shot basis. This contribution of the arc current falls off as we go up in frequency because of the decreasing amplitude of the Fourier components of the arc current pulse. The other contribution to the noise from the unshielded test set comes from the trigger in the gap switch, and the initial electrical breakdown in the gap switch.

The test set developed represents an excellent device to operate the thruster in air. However, it is quite clear from noise measurements made of the unshielded device that a shielding analysis will be required to reduce the noise level of the test set to within acceptable limits. Since the present study presents the amplitude and frequency variation of the noise of the basic test set, it is now possible to perform a meaningful shielding analysis of the test set. It should be noted that the use of high permeability material will probably be required to shield the test set against the low frequency magnetic fields.

4.1.3 Thruster Enclosure Shielding Tests

Testing of the shielding effectiveness of the thruster enclosure* was carried out in a shielded room. The receiver was located in the same room with the thruster enclosure. The sources that were used to excite the antenna within the otherwise empty thruster enclosure were located outside the test room in another shielded room that was configured with the main room. A metal wall separated the two rooms. The thruster enclosure was mounted on the wall via a metal pipe. The pipe was used to pass the cables into the enclosure. Figure 29 is a schematic diagram of the set up.

In the set up shown in Figure 29, the thruster enclosure becomes an extension of the shielded room that contains the signal source.

The shielding effectiveness of the thruster's enclosure was determined in the following manner. The field was measured first with one of the thruster enclosure covers removed. The cover that was removed faced the receiving antenna. This cover was then replaced and the field was measured. The difference in field strength observed is denoted as the shielding effectiveness of the enclosure. In this test we attempted to keep the power level to the transmitting antenna constant. This shielding effectiveness test was performed with and without metal gaskets in the cover plates of the thruster

* It should be noted that the basic thruster was removed from its enclosure that was being evaluated in these tests. The exhaust cone was also removed and a cover plate with gasket was used to cover up the exhaust cone opening in the thruster enclosure.

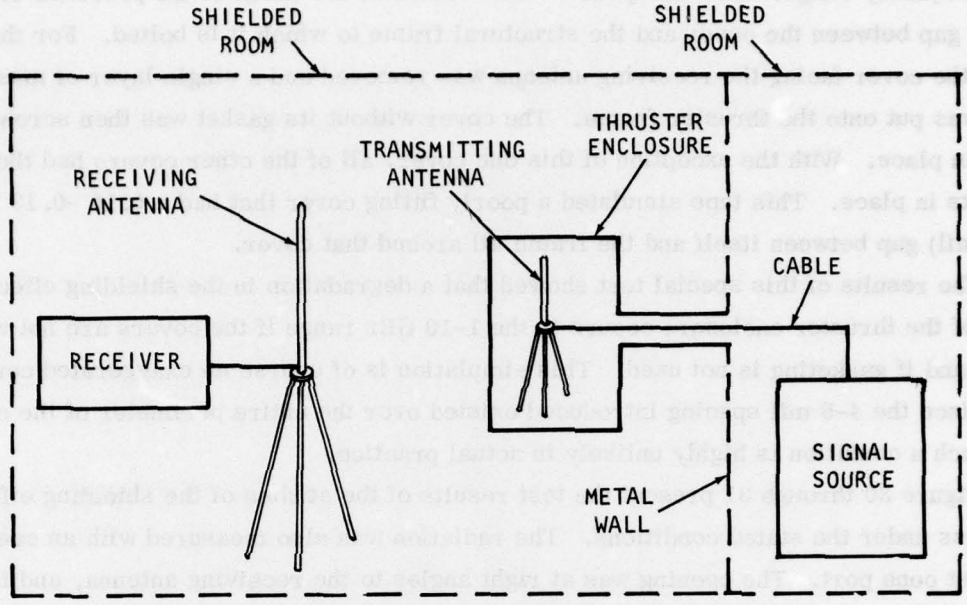

Figure 29. Laboratory Set Up For Shielding Effectiveness Test

enclosure. The frequency range that was examined covered the same range as the unshielded test set noise tests. Early in the testing, it became clear that the level of magnetic excitation would be higher than the electric excitation at the same frequency. Since magnetic excitation yields conservative results compared to electric excitation, we did not pursue electric excitation measurements at frequencies less than 25 MHz. At the higher frequencies, electric excitation was used, but it was not possible to obtain a dynamic range which was greater then 60 db, except at 172 MHz where a 72 db change was achieved with and without the covers. It should be emphasized that for the electric excitation being discussed this result is a lower bound on the shielding effectiveness. The reason for this is that the signal, for electric excitation, disappeared into the receiver noise when the cover was put back on the enclosure.

In the 1-10 GHz range, a T.W.T. was used to excite the antennas. The shielding effectiveness was again measured with and without gaskets. Since we could not effectively

excite the antennas in the mid range, we substituted another independent test for the mid frequency range. This independent test examined the effect of the presence of a small gap between the cover and the structural frame to which it is bolted. For this test, the cover facing the receiving antenna was removed and a single layer of masking tape was put onto the thruster frame. The cover without its gasket was then screwed back in place. With the exception of this one cover, all of the other covers had their gaskets in place. This tape simulated a poorly fitting cover that had a 0.10 -0.13 mm. (4-5 mil) gap between itself and the frame all around that cover.

The results of this special test showed that a degradation in the shielding effectiveness of the thruster enclosure occurs in the 1-10 GHz range if the covers are not well fitted and if gasketing is not used. This simulation is of course an exaggerated condition since the 4-5 mil spacing introduced existed over the entire perimeter of the cover, and such a condition is highly unlikely in actual practice.

Figure 30 through 31 present the test results of the studies of the shielding effectiveness under the stated conditions. The radiation was also measured with an open exhaust cone port. The opening was at right angles to the receiving antenna, and faced the ceiling of the shielded room. The frequency range of these measurement encompassed

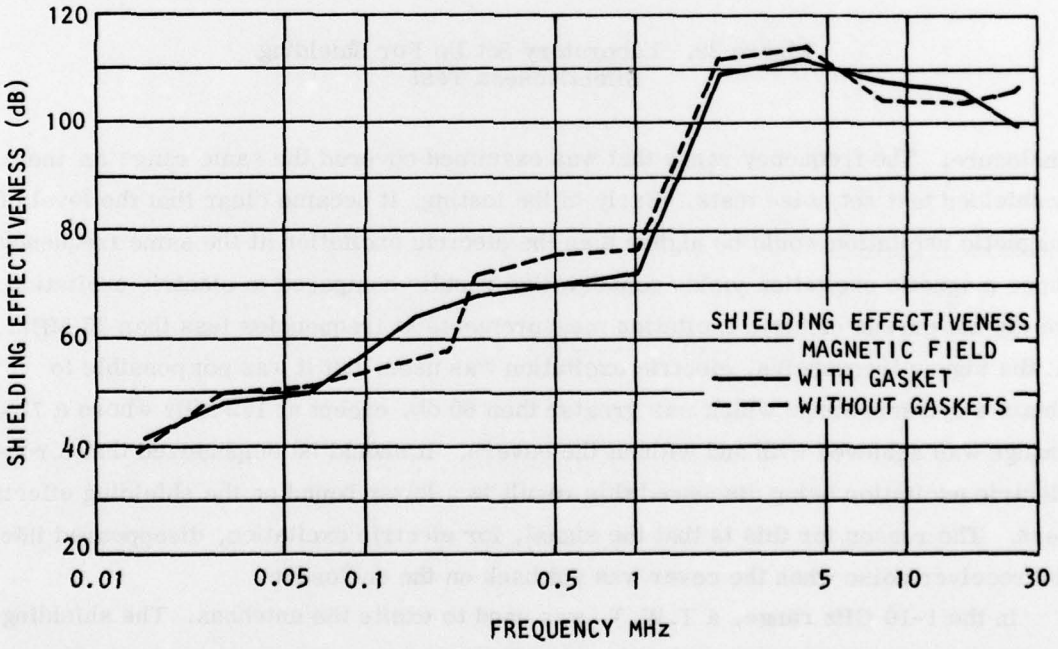

Figure 30. Shielding Effectiveness (Magnetic Field, 15 KHz - 30 MHz)

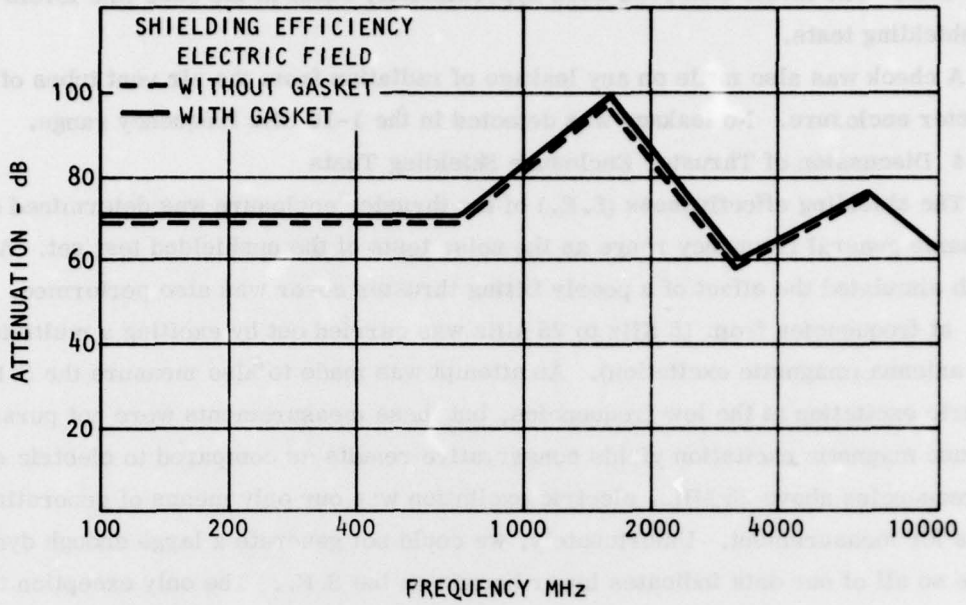

Figure 31. Shielding Effectiveness (Electric Field, 100 MHz - 10 GHz)

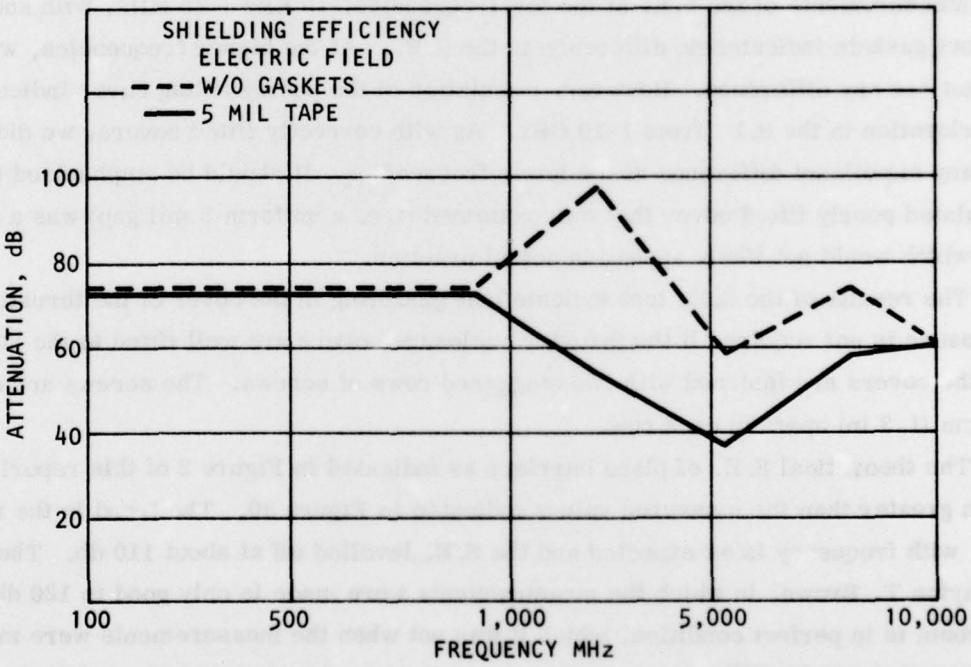

Figure 32. Shielding Effectiveness (Electric Field, 100 MHz - 10 GHz)

1-10 GHz. The levels observed were approximately equal to the base line levels used for the shielding tests.

A check was also made on any leakage of radiation from the air vent tubes of the thruster enclosure. No leakage was detected in the 1-10 GHz frequency range.

4.1.4 Discussion of Thruster Enclosure Shielding Tests

The shielding effectiveness (S.E.) of the thruster enclosure was determined over the same general frequency range as the noise tests of the unshielded test set. A test which simulated the effect of a poorly fitting thruster cover was also performed. The S.E. at frequencies from 15 KHz to 25 MHz was carried out by exciting a multi-turn loop antenna (magnetic excitation). An attempt was made to also measure the S.E. using electric excitation at the low frequencies, but these measurements were not pursued because magnetic excitation yields conservative results as compared to electric excitation. At frequencies above 25 MHz, electric excitation was our only means of generating the fields for measurement. Unfortunately, we could not generate a large enough dynamic range so all of our data indicates lower bounds on the S.E.. The only exception to this is the simulation of a poorly fitting cover. In this case, enough leakage was present to actually measure the S.E..

Measurements of the S.E. at the low frequencies, 15 KHz - 25 MHz, with and without gaskets indicates no difference in the S.E.. At the higher frequencies, we also did not see any difference. However, simulation of the poorly fitting cover indicated a deterioration in the S.E. from 1-10 GHz. As with correctly fitted covers, we did not see any significant difference at the lower frequencies. It should be emphasized that the simulated poorly fitted cover that was examined (i.e. a uniform 5 mil gap) was a condition which would not likely appear in actual practice.

The results of the S.E. test indicate that gasketing in the cover of the thruster enclosure is not required if the thruster enclosure covers are well fitted to the structure and the covers are fastened with two staggered rows of screws. The screws are spaced 3.4 cm (1.3 in) apart in each row.

The theoretical S.E. of plane barriers as indicated in Figure 2 of this report are much greater than the measured values indicated in Figure 30. The trend in the measured S.E. with frequency is as expected and the S.E. levelled off at about 110 db. The room at Dayton T. Brown, in which the measurements were made is only good to 120 db when the room is in perfect condition, which it was not when the measurements were made. The greatest single difficulty encountered was the interface between the room where the

measurements were made and the adjacent room where the excitation equipment was located. It is probably a fact that the limit of the room as indicated in Figure 30 is 110 db.

As mentioned above, the low frequency data shows the S. E. increasing with increasing frequency. We believe that the measured values of the S. E. should be closer to the theoretical values. The effect of gasketing as indicated in Figure 30 is as expected, since the gaskets are made of aluminum wire. Another limitation of the measurement was our inability to accurately monitor the power into the antennas with and without the covers on. One would suspect that if antenna loading occurred then we would be measuring shielding numbers which are too high. This would imply that the box leaked. However, we do not believe that the box had any substantial leaks. This possibility was checked by probing with an antenna around the box. This technique revealed a leak only when the 4-5 mil thick tape was put around the perimeter of one of the covers to simulate a poorly fitting cover.

In all probability, both the equipment and our measurements were not adequate to accurately measure the S. E. as a function of frequency, and that the absolute values of S. E. as a function of frequency are not reliable. However, we do believe that our comparisons of S. E. with and without gasketing are reliable as was the simulation of a poorly fitted cover.

5.0 THRUSTER DESIGN CONSIDERATIONS AND PERFORMANCE

During the design analysis phase of the thruster two design approaches were considered. One of these sought techniques to minimize EMI emissions from the edges of the electrical stripline of the thruster and also through the teflon propellant rods entering the sides of the electrode nozzle. The second design approach considered fully enclosing the thruster in an EMI secure structural housing to contain any possible emissions within the enclosure. This second approach was considered the better of the two approaches. Furthermore, with this latter approach it would also be possible to utilize all design data and techniques of the present efforts to all future systems. The basic thruster design was therefore left essentially the same as reported in Reference 5.

In order to have the thruster exhaust cone represent an extension of the thruster enclosure, it was necessary to perform a minor redesign of the exhaust cone. The exhaust cone was fabricated of aluminum and Mykroy insulation was used to cover the aluminum cone. However, an aluminum flange was provided on the outside of the exhaust cone to electrically interface the aluminum cone directly to the enclosure which

surrounded the thruster. The geometry of the thruster exhaust cone puts it into the class of a pyramidal horn. It was not possible to determine cone geometry modifications, if any, which could be provided to the present geometry in order to reduce side lobes of radiation. Whether or not the computer analysis reported in Reference 6 could be used for a pulsed plasma thruster could not be established.

The basic frame for the enclosure (see Figure 1) was fabricated of aluminum angle. After welding the frame, it was machined to achieve the required dimensional tolerance sought. Gasket grooves were machined into all of the covers of the enclosure as well as into the flange of the exhaust cone. To realize vacuum compatible gasketing, an aluminum weave gasket was selected without fillers. Problems were encountered in procuring such gaskets to the dimensional tolerances requested. The density of the knit was found to be a very important parameter in specifying the gasket. Gaskets were finally obtained which, with a minimum of 5 psi compression would fit within the machined grooves of the lids.

Electrical and instrumentation feed-throughs were required in the thruster enclosure in order to allow thruster operation and monitoring of the system temperature. To confine EMI noise within the enclosure it became necessary to select EMI secure feed-throughs and filters. Figure 33 presents a schematic of the entire system, including the external test set, which was used during the program. In order to use the thruster igniter plug pulse as the input trigger for the spark gap switch of the external test set, provisions were provided to divert the igniter plug pulse. The approach used was to pass the thruster igniter plug pulse from within the housing via an external loop back into the housing. This loop could easily be externally diverted from the igniter plug to the external test set. Tri-axial cable and bulkhead feedthroughs were used for this purpose. This loop can be seen in Figure 1 to be located to the right side of the rear handle on the top cover of the housing. The filtered thermocouple feedthroughs are on the left side of the same cover (see Figure 1).

The propulsion performance of the thruster was measured on a thrust balance while operating in a vacuum chamber. The result of two tests are presented in Table 3.

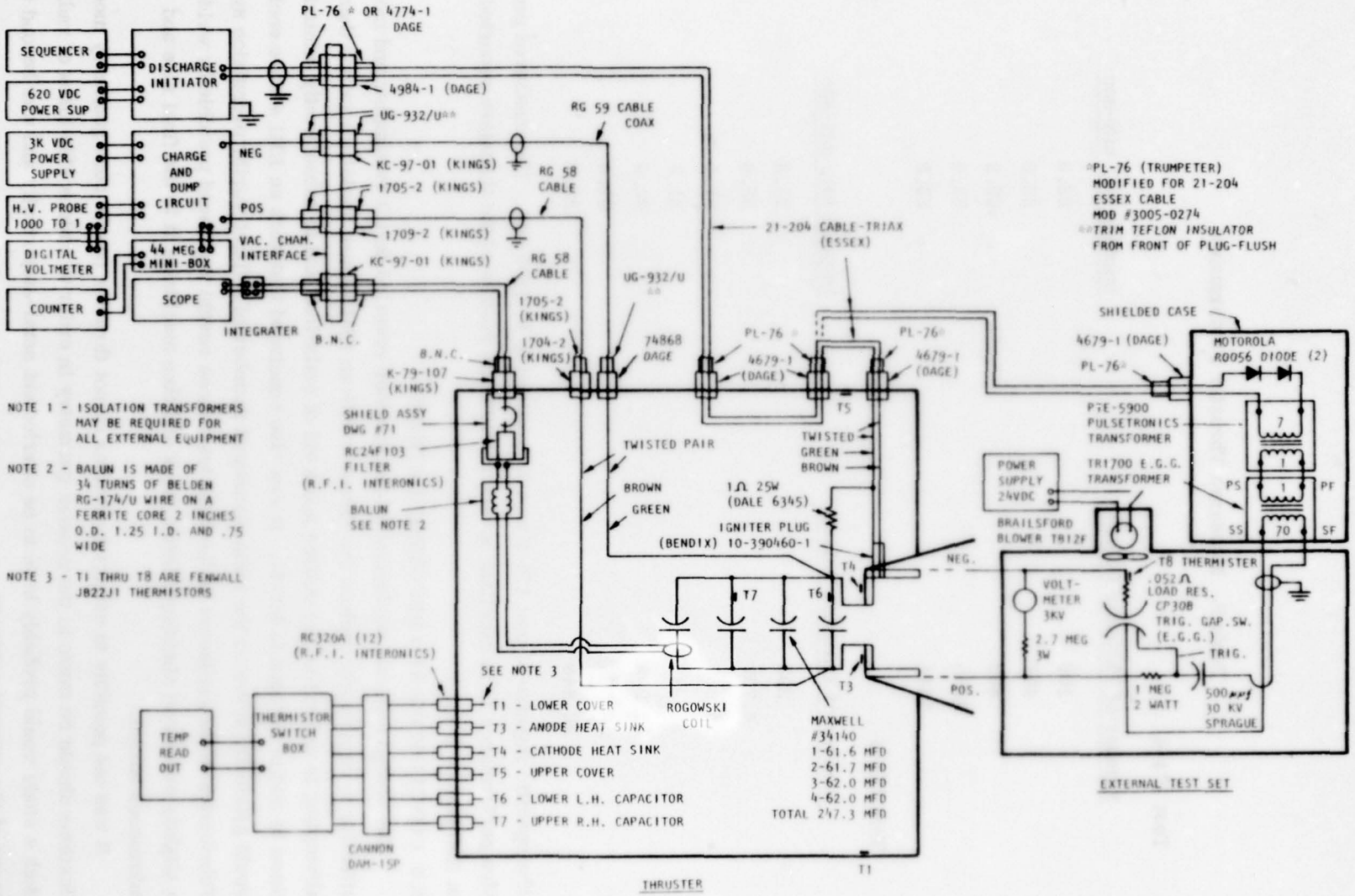

Figure 33. Schematic of Entire System

Table 3. Measured Thruster Performance

Test 174-4

Number of Thruster Pulses	Impulse bit, mN-sec
100	22.8
497	23.5
802	23.2
1255	23.6
1644	23.8

Test 174-9

Number of Thruster Pulses	Impulse bit, mN-sec
293	23.8
4,737	23.6
15,869	21.5
21,237	21.2
31,993	21.5
36,556	21.9
96,448	23.6

The specific impulse of test 174-9 was determined to be 1679 sec. The measured propulsive performance is in excellant agreement with the results of the thrusters reported in References 5 and 7.

6.0 CONCLUSIONS AND RECOMMENDATIONS

The design analysis performed of the thruster revealed that it is simpler and more effective to completely enclose the thruster with an EMI secure enclosure rather than attempting to determine the source and level of emissions and to subsequently minimize these to within acceptable levels. It was also concluded that such an EMI secure enclosure would generally serve as the main structural member of a flight worthy propulsion system. Fabrication of the enclosure to the tight tolerances sought was found possible by welding a slightly oversized aluminum frame work and then machining it to the final size and tolerances sought.

It was not possible to establish whether or not thruster nozzle cone geometry modifications should be made to the present geometry in order to reduce side lobes of radiation. Such a study would probably have to be carried out semi-empirically and was beyond the scope of the present program.

Electrically interfacing the external test set to the thruster electrodes was found to be greatly simplified by providing accessible screwholes in the electrodes of the thruster and bolting thin flexible electrode extensions of the switch of the external test set to the thruster electrodes. Such an electrical connection could be made without disconnecting the exhaust cone of the thruster and without putting an undue mechanical stress on the thrusters electrode assembly.

It was found possible to use the thruster's high voltage ignition pulse as the electrical input to trigger the switch of the external test set in a safe and EMI secure manner if the igniter plug lead of the thruster is interrupted by a removable loop of triaxial cable. Locating this loop outside of the thruster enclosure near the thruster nozzle allows the thruster ignition pulse to be safely diverted to the external test set whenever the test set is connected to the thruster. This technique prevents the igniter plug of the thruster from accidentally becoming energized when the test set is being used.

Of the approaches examined, it was concluded that the use of a step-down transformer located in the external test set to reduce the thrusters diverted high voltage ignition pulse to the desired level provided the most reliable and reproducible trigger input signal to the external test set.

The unshielded external test set developed in this program allowed the thruster to be repetetively operated in air. However, it is necessary to cool the resistive load of the test set by a small electric fan. The present design provides a slightly oscillating discharge with a peak current of about 47 kiloamperes. The peak current is lower than that generated by the thruster without the test set attached to it.

During spacecraft integration tests it might be desirable to have a test set which can also be used in a thermal-vacuum environment. It is believed that the present electrical design of the external test set could be used in such an environment. However, it would be necessary to replace the present air cooled resistor with one which can be conductively cooled.

The electromagnetic noise generated by the unshielded test set does not meet the requirements (para. 5.1.2.1.4) of MIL STD 1541 for broad band magnetic noise nor does it meet the requirements of MIL STD 461 (RE02) for broad band electric field noise. The largest noise signal occurs in front of the test set and the smallest signal occurs when the thruster enclosure is located between the test set and the receiving antenna. If a user desires to operate the test set within the limits of the above cited specifications, it will be necessary to provide electromagnetic shielding. The measured noise can then serve as a basis for the design of a shielded enclosure to be fitted around the test set.

The shielding effectiveness measurements revealed that gasketing is not required for the covers of the thruster enclosure if they are well fitted and provided by a double row of alternately spaced screws.

It has been concluded that the equipment used and measurements made did not provide an accurate measurement of the absolute value of shielding effectiveness as a function of frequency. However, the comparison of the relative shielding effectiveness with and without gasketing is considered to be correct.

It is recommended that in future tests the power into the antennas be measured with and without thruster covers in order to check antenna loading.

7.0 REFERENCES

1. Palumbo, D.J., Begun, M., Guman, W.T. - Pulsed Plasma Propulsion Technology, Interim Report AFRDL-TR-74-50, Air Force Rocket Propulsion Laboratory, Edwards, Calif., 1974
2. Stratton, Julius A. - "Electromagnetic Theory", McGraw Hill, N.Y. 1941, Pg. 436-437
3. White, Donald R.J. - "Electromagnetic Shielding Materials and Performance", Don White Consultants, Inc., Germantown, Maryland, 1975
4. Collins, R.E. - "Field Theory of Guided Waves" McGraw Hill, N.Y., 1960, Pg. 197
5. Guman, W.J., Begun, M., Pulsed Plasma Plume Studies, Report AFRPL-TR-77-2, Air Force Rocket Propulsion Laboratory, Edwards, Calif., March 1977.
6. Loeter, G.N., Newton, J.M., Schuchardt, J.M., Dees, J.W., "Computer Analysis Speeds Corrugated Horn Design", *Microwaves, pp 58-65, May 1976*
7. Palumbo, D.J., Guman, W.J., "Pulsed Plasma Propulsion Technology", AFRPL-TR-77, Air Force Rocket Propulsion Laboratory, Edwards, Calif., 1977